







Cite this: *J. Mater. Chem. C*, 2019, 7, 12761

Solution-processable electrochromic materials and devices: roadblocks and strategies towards large-scale applications

Xuefei Li,  † Kuluni Perera,  † Jiazhi He, Aristide Gumyusenge  and Jianguo Mei  *

Electrochromic devices (ECDs) that modulate optical transmission or reflection in a controllable manner are attractive in energy-saving and colour-tuning applications. In this review, we discuss the key components, fundamental working principles and performance metrics of ECDs using layman's terms. We also highlight recent materials development of each component and illustrate how the structure–property relationships impact their processability, device performance and stability. We further introduce emerging materials that exhibit electrochromic properties, and discuss the transition from laboratory-scale, half-cell-based characterisations of electrochromic materials to the fabrication of solid-state electrochromic devices and evaluation of their performances. Finally, we lay out major challenges for fabricating large-scale and cost-effective ECDs, particularly the materials design and fabrication strategies for achieving chemically and electrochemically stable, high performance ECDs that can be produced by roll-to-roll techniques.

Received 28th May 2019,
Accepted 22nd July 2019

DOI: 10.1039/c9tc02861g

rsc.li/materials-c

1. Introduction

Electrochromic materials that reversibly modulate optical transmittance or reflectance under applied potentials are key components for a variety of energy saving and colour-tuning applications,¹ especially when integrated into “smart windows” that switch between a coloured (dark) state and a colourless

(bleached) state to increase energy efficiency of buildings,² or colour-tuning mirrors that adaptively modulate reflection based on ambient light conditions.³ Since the initial reports of electrochromism in WO_3 ,^{4,5} intensive research efforts have been focused on electrochromic materials of various categories, including transition metal oxides,^{6,7} small molecules^{8,9} and polymers.^{10,11} Other device components, including the ion storage layer (counter electrode), electrolyte, and conductive substrates, are also prerequisites for achieving functional solid-state devices with desired performance and stability. Meanwhile, the availability of large-scale processing techniques

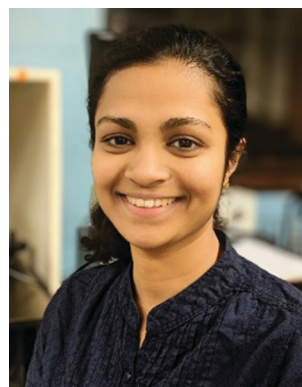
Department of Chemistry, Purdue University, 560 Oval Dr., West Lafayette, IN 47907, USA. E-mail: jgmei@purdue.edu

† Equal contribution.



Xuefei Li

Xuefei Li obtained her PhD in Chemistry in 2019 at Pennsylvania State University, under the supervision of Professor Raymond E. Schaak. Her graduate work focused on the synthesis and metal–insulator transition properties of vanadium dioxide nanostructures. She is currently a postdoctoral research fellow in the laboratory of Professor Jianguo Mei at Purdue University, focusing on the synthesis and application of inorganic nanomaterials for electrochromic devices.



Kuluni Perera

Kuluni Perera obtained her BSc in Chemistry in 2016 at the University of Colombo, Sri Lanka. She is currently a graduate student in Professor Jianguo Mei's lab at Purdue University. Her research interests include electrochemistry of conjugated polymers and polymer thin film energy devices.

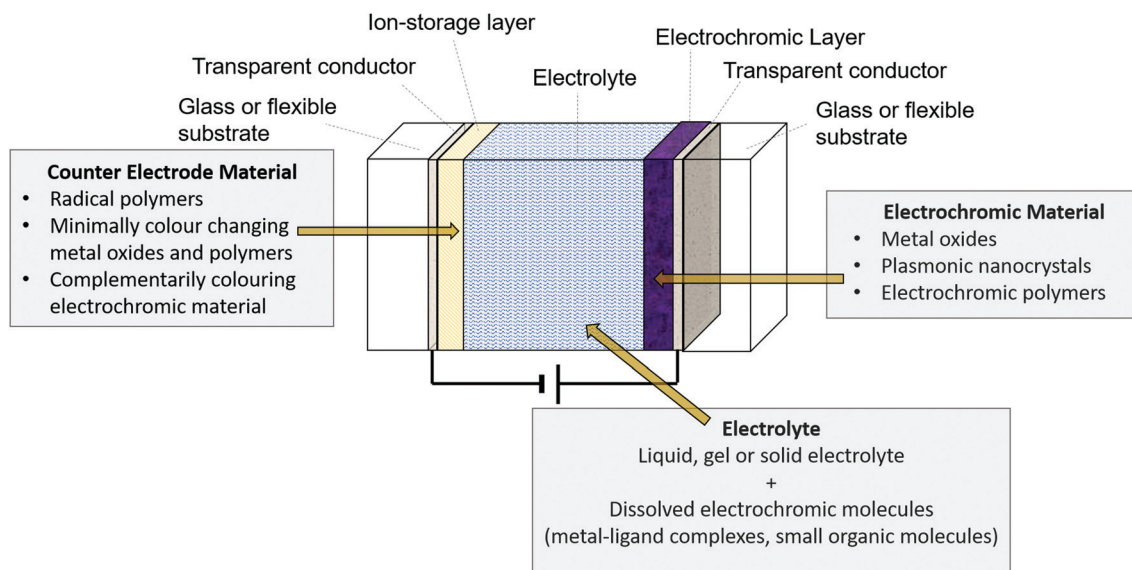


Fig. 1 Schematic representation of a transmissive type electrochromic device (ECD), composed of electrochromic material, electrolyte and counter electrode material sandwiched between transparent conductive substrates.

including roll-to-roll coating are key to the integration of these components into economically-attractive commercial devices.

In this review, we focus on the materials used for different components of an electrochromic device, highlighting their performance metrics, processability and advances in roll-to-roll processing, together with the remaining roadblocks and potential strategies that can be used for achieving large-scale fabrication of all-printed devices. Several classes of electrochromic materials, including transition metal oxides, plasmonic doped metal oxides, electrochromic polymers, and emerging classes of materials exhibiting electrochromic properties are presented, focusing on the technological challenges associated with the synthesis, fabrication and assembly using large-scale processing techniques. We then discuss materials for counter electrodes, electrolytes, and conductive substrates, review their chemical and electrochemical stability, and analyse how

each component can be compatible with roll-to-roll coating techniques. We conclude by highlighting a few major hurdles that need to be addressed as we move to develop roll-to-roll manufacturing of ECDs.

2. Electrochromic device structures

The working mechanism of an electrochromic material involves colour changes induced *via* an electrochemical process. Formally defined, electrochromism is a reversible change, evocation or bleaching of a material's colour through an electron transfer process (redox reaction) or application of a sufficient electrochemical potential.¹² In its simplest form, a device incorporating such an electrochromic material requires a working electrode at which the active material undergoes electrochromic switching, a counter electrode that functions as a charge balancing and/or ion storage layer, and an electrolyte maintaining ionic transport between the two electrodes, to form an electrochemical cell. The observed colour changes are a result of the redox events occurring in the ECD.

ECDs are constructed based on two major device architectures: the layered arrangement (sandwich configuration)¹³ or the "all-in-one"¹⁴ approach. In the layered structure, the electrochromic material is coated on a conductive substrate as the working electrode, and the electrolyte and ion-storage material form distinct layers (Fig. 1).¹⁵ Alternatively, instead of preparing separate films or layers, readily soluble electrochromic molecules can be dissolved in the electrolyte together with a redox mediator in the "all-in-one" configuration.^{16,17}

In terms of large-scale processing, the distinct layers in the sandwich configuration can be separately prepared using different coating techniques and assembled together to form the final device structure through roll-to-roll techniques. Advantages of this device architecture include the independent



Jianguo Mei

Jianguo Mei is currently an Assistant Professor of Chemistry at Purdue University. He has published over 70 peer-reviewed papers with over 8500 citations, 4 book chapters and 6 granted US patents. Dr Mei is a recipient of an NSF CAREER award, Office of Naval Research Young Investigator award (ONR YIP) and Purdue's Teaching for Tomorrow Fellowship. He is also a co-founder of Ambilight Inc, a venture-backed start-up company

dedicated to the commercialization of roll-to-roll manufactured thin-film electrochromics for smart windows.

optimisation of processing conditions of individual layers and the broad versatility of using any type of solid-state electrochromic material to obtain uniform electrochromic switching even in large-area devices. On the other hand, only small molecules or metal–ligand complexes with high solubility in the electrolyte can be employed in the “all-in-one” construct. Depending on the specific application, ECDs can be fabricated either in a transmissive or reflective configuration.¹⁸ Transmissive devices controllably tune light transmission, and are useful as smart windows,¹⁹ non-emissive displays,^{17,20,21} eye-wear²² and optical shutters.²³ They function by altering the amount of light transmitted in a given wavelength range in response to an applied voltage, switching between different colours or between a coloured and a transmissive state. Reflective-type devices are commercially used in the auto-dimmable Gentex Night Vision System (NVS) anti-glare rear-view mirrors,²⁴ and are also studied for potential applications in thermal control through reflectance modulation in the infrared (IR) region as well as for display applications.^{25–28} The major difference of the two device configurations is the choice of conductive substrates. The transparent substrate used in transmissive-type devices is typically replaced by a reflective surface in a reflective-type device. Occasionally, the electrochromic layer on the reflective surface may face outwards, relying on slits or pores on the conductive surfaces to establish the electrical connection with the electrolyte.^{11,29}

3. Characterisation and performance metrics

The main feature identifying an electrochromic material is the ability to change its optical properties in response to an external electrical bias. As implied from its basic function, techniques related to both electrochemistry and optical spectroscopy are required to fully evaluate the performance of a given material as a potential candidate for electrochemically induced colour attenuation applications. A high-performance ECD is capable of manifesting fast, reversible and controllable optical modulations of high contrast, with chemical and electrochemical stability. As the field grows, it becomes increasingly challenging to compare reported performances of materials and devices using ambiguously defined performance metrics. Thus, several critical performance metrics used to characterise EC performance of a material are highlighted below. We encourage the community to provide a standardised performance measurement for the evaluation of new electrochromic materials for specific applications.

3.1 Electrochemical properties

The first step in characterising the electroactivity of an electrochromic material is to understand the electrochemical processes that give rise to reversible electrochromic switching. The initial step of electrochemical characterisation is usually carried out using a three-electrode setup, where the material of interest is either coated on the working electrode or kept dissolved in the electrolyte. The material's redox properties can be understood

using cyclic voltammetry (CV) experiments, where the current response is recorded as a function of varying voltages by performing forward and reverse scans within a specified voltage range at a given rate.³⁰ During the initial scan from lower to higher potentials (or *vice versa*), the material undergoes a capacitive charging process, and is typically accompanied by a faradaic electron transfer corresponding to the oxidation (or reduction) of the material. During the reverse scan the discharging and the opposite redox events occur. For certain EC materials such as plasmonics, only an increase or decrease of the free carrier concentration is required to cause the capacitive electrochromic phenomenon.^{31,32} From the voltammograms, the reversibility of the compounds upon oxidation or reduction can be evaluated *via* the analysis of the peak-to-peak separation, the ratio of the peak current densities, the peak current density *versus* the scan rate or square root of the scan rate, *etc.*³³ Materials that undergo readily reversible oxidations are referred to as “p-type” materials and those that prefer reductions are called “n-type”. The terms “anode-active” and “cathode-active” are also used interchangeably to describe the above phenomena.

In an electrochromic device, the current responsible for inducing the colour change (I) can be represented as follows:

$$I = \frac{V_e}{R_t} = \frac{[V_a - (\phi_{IS} - \phi_{EC}) - V_b]}{R_t} \quad (1)$$

where V_e = effective colouring voltage, V_a = applied voltage, V_b = sum of all interface barrier potentials, ϕ_{IS} and ϕ_{EC} represent the internal chemical potential differences of the ion storage layer and the electrochromic layer, respectively, and R_t = sum of resistances to the electronic and ionic currents in the complete system.³⁴ The effective voltage (V_e) and resistance values are influenced by the choice of materials, the thicknesses of the electrochromic and ion storage layers, as well as the charge and mobility of the electrolyte ions.

It is clear from eqn (1) that the application of an overpotential (greater than the voltage V_e , required for the colour change) is necessary to overcome the barrier potentials present in the system. However, overpotentials may also lead to deterioration of the electrochromic materials and irreversible side reactions. Therefore, it is important to identify a “safe” voltage range for an ECD by considering the electrochemical stability of the electrochromic layer,^{35,36} as well as the other materials used in the device.³⁷ A stable operating voltage window can be defined as the potential range in which the electrochromic material undergoes reversible electrochemical redox reactions (pertaining to the colour change), in the absence of irreversible side reactions involving the other components of the ECDs, namely the ion-storage layer, electrolyte and conductive substrates. The limiting potentials required for complete and reversible switching of the device, should lie within the stability window of the electrolyte.³⁸ The electrochromic potential window of the device, which is the potential range where the colour change occurs,³⁹ can be readily determined through spectroelectrochemistry (described in the following section), while the electrochemical stability and reversibility of the redox reactions of active materials are estimated by

comparing changes in the peak positions, peak-to-peak distance and current densities of the forward and reverse scans of a cyclic voltammogram.

A few approaches have been developed to prevent the use of excessive switching voltages for a given pair of electrochromic and ion storage layers, in order to increase the device lifetime and improve compatibility with different electrolyte systems. Of significant interest is the use of electrodes with unbalanced redox capacities in an ECD.⁴⁰ By using an ion-storage layer with a substantially higher redox capacity with respect to the electrochromic layer, only partial switching of the ion-storage material is required to balance the charge generated at the working electrode corresponding to a complete switch of the electrochromic material. Circumventing the requirement for complete switching of one active layer enables narrowing of the voltage window. Elevated temperatures have proven to decrease the voltages required for the colouring and bleaching of metal-oxide materials by improving charge transfer and ionic diffusion processes.⁴¹ Diffusion coefficients of ions are exponentially related to temperature, therefore a slight increase in temperature can significantly increase ionic diffusion, resulting in lower colour changing voltages.⁴² Especially in the case of diffusion-limited systems, such as those containing solid-state electrolytes, improving the ionic conductivity in the electrolyte and decreasing the interfacial barriers for ion intercalation-deintercalation by engineering thinner, more porous electrolyte layers have shown to be beneficial for obtaining smaller operating voltages.³⁴

Apart from cyclic voltammetry, other electrochemical techniques, including chronoamperometry and chronopotentiometry can be used to track the charging/discharging process of the electrochromic device.^{43,44} Electrochemical impedance data are useful in determining the ionic mobility of the electrolyte, charge transfer processes and resistive barriers present in the system.

3.2 Spectroelectrochemistry

Spectroelectrochemistry is a technique used to monitor a material's spectroscopic changes that occur during electrochemical experiments (Fig. 2). It enables characterisation of

single/multiple electron transfer processes and tracking the generation of intermediate species during the redox processes by identification of their unique spectral features.⁴⁵ Spectroelectrochemistry is used as a tool to determine the evolution of colour spectra of an electrochromic material, and to assess the potential of a material to achieve a certain colour.^{46–48} With the aid of spectroscopic data, the scope of application is decided (e.g. coloured to bleached transitions, multi-coloured electrochromism or minimal-colour change). For example, *N*-alkyl-substituted poly(3,4-propylenedioxyppyrrrole) (PProDOP), which has a low colouration efficiency was studied by Reynolds *et al.*⁴⁹ The neutral state of the *N*-alkyl-substituted PProDOP has a band absorption below 400 nm, and in intermediate oxidised states the absorption shifts to ~500 nm, and finally ends in the near IR (NIR) region, with minimal colour residue in the visible region. Owing to the unique spectroelectrochemical behaviours, *N*-alkyl-substituted PProDOP was identified as a candidate for counter electrode materials (described further in Section 5).

3.3 Colour analysis

Colour is a core aspect of electrochromics, as these materials and devices function as attenuators of visual stimulation, in the form of colour-changing displays,^{17,20,21} dynamic eye-wear,²² active camouflage materials or switchable windows and mirrors.^{3,19} Especially when considering visual comfort levels or commercial applications such as advertising and interior lighting, stringent colour requirements are often imposed. Since colour perception is a subjective matter, internationally accepted colour descriptions are required to confirm the extent of colour matching of the electrochromic material with the expected standards.⁵⁰ Colorimetry (colour measurement) enables a scientific quantification and a standardised description of colour by mathematically simulating the perceived colour. "Colorimetric analysis" is usually performed according to protocols set out by the International Commission on Illumination (CIE, Commission Internationale de l'Éclairage), that delineate methods to represent the three main attributes that define

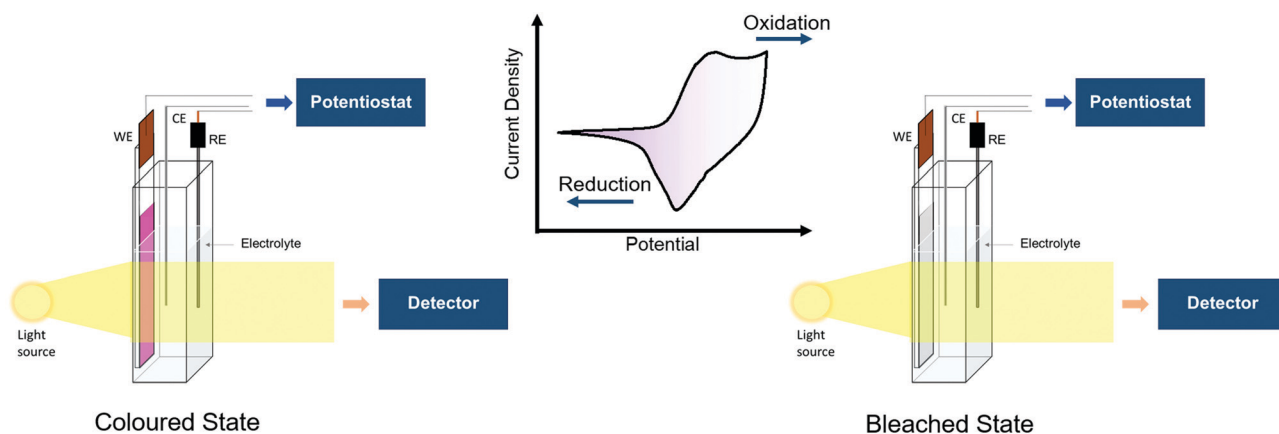


Fig. 2 Schematic representation of a three-electrode spectroelectrochemical setup consisting of a working electrode (WE), a reference electrode (RE) and a counter electrode (CE). Changes in optical properties (e.g. coloured to bleached transitions) corresponding to electrochemical processes (oxidation or reduction) can be recorded *in situ*.

a colour: hue, saturation and lightness. Hue refers to the dominant wavelength or spectral position of the light associated with the colour, and it can be represented by its position on a colour wheel or spectral axis. In simple terms, this feature helps to identify the colour as red, blue, green, yellow, orange, *etc.* The level of saturation describes how close the observed colour is to the pure spectral colour, and if it is mixed with any forms of grey, *i.e.* desaturated. This feature is sometimes also known as the “tone” of a colour. The amount of brightness or luminosity is considered the third attribute.^{51,52}

Colour spaces which represent all possible colours in an organised manner are constructed based on the tristimulus values (XYZ).⁵³ The XYZ values are analogous to the sensitivity of the cone cells present in the human eye, which are responsible for detecting long, middle and short wavelength radiation. CIE 1931 Yxy ⁵⁰ and 1976 CIE $L^*a^*b^*$ ¹¹ are two such frequently used colour spaces. The $L^*a^*b^*$ system is widely used in the electrochromic industry, as it has better numerical correlation with visually observed colour changes.⁵⁴ In this three-dimensional colour space, L^* axis represents lightness (ranges between values of 0 and 100), and a^* and b^* axes denote chromaticity (Fig. 3). $+a^*$ values indicate colours with rich red hues, $-a^*$ values green shades, and the b^* axis represents yellow ($+b^*$) and blue ($-b^*$). The (0,0) point in the a^*b^* coordinate system represents a neutral (achromatic) grey.^{55,56} Calculations based on these $L^*a^*b^*$ values can be used to represent the colour differences (ΔE) with respect to a reference.^{51,57,58}

Frequently, electrochromic materials are mixed with each other, or together with other dyes or pigments to create new

shades or tones to extend the accessible colour gamut. Since electrochromics are typically used in non-emissive devices, the subtractive theory of colour mixing, based on cyan, magenta and yellow (CMY) as primary colours, is useful in predicting the colour of mixtures. Appropriate combinations of the three primaries are used to create black.⁵⁹ On the other hand, if combinations of transmitted light need to be considered, the additive theory based on RGB (red, green and blue) primary colours would be required.

3.4 Optical contrast

Optical contrast refers to the degree of optical change during the switching process, and it is commonly expressed in one of the following correlated forms: a change in optical density (ΔOD), transmittance ($\Delta \%T$), reflectance ($\Delta \%R$), or relative luminance ($\Delta \%Y$). All four measurements are a variable as a function of wavelength. In a given instance, the choice of measurement type to best represent the electrochromic contrast depends on the optical properties of a material and the intended application. Optical density changes (measured in the form of absorbance) are reported for materials exhibiting coloured to bleached transitions as well as for dual and multi-coloured electrochromics. However, for materials switching between coloured and highly transmissive states, the standard approach is to measure relative transmittance changes ($\Delta \%T$) at λ_{\max} (the wavelength at which the material shows maximum optical change). As opposed to transmissive devices, reflective systems (with low transmittance) track modulations in diffuse reflectance. The transmission or reflectance changes are

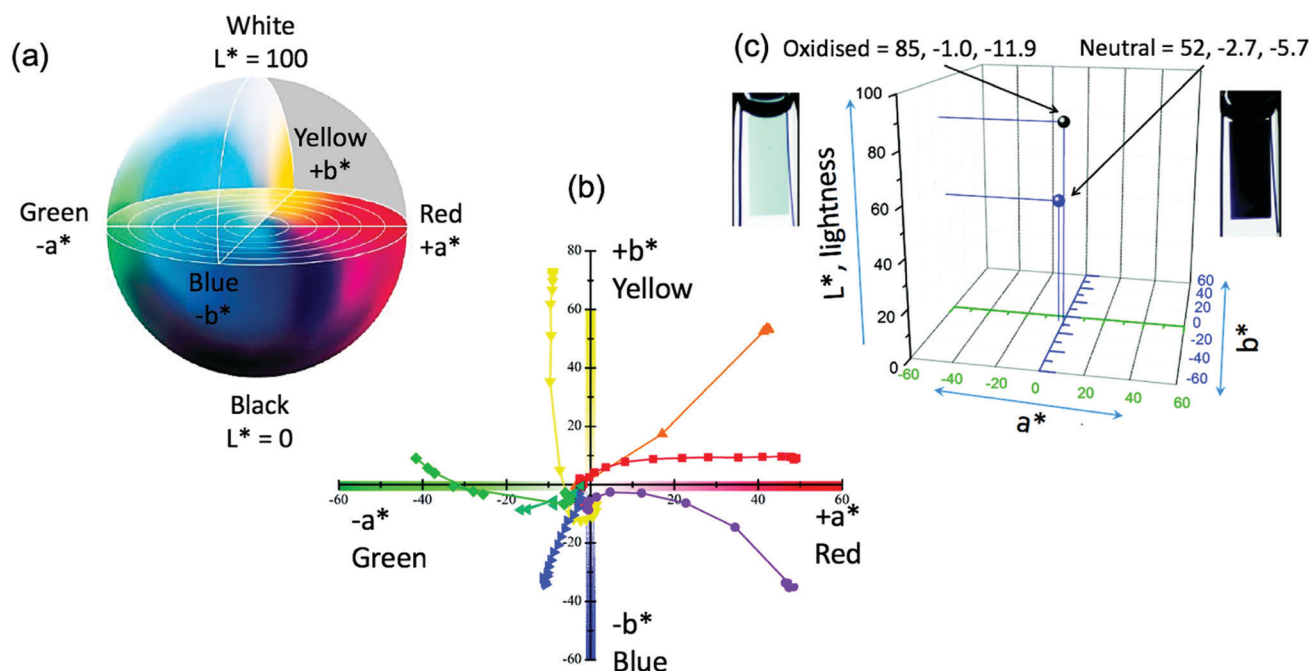


Fig. 3 (a) 1976 CIE $L^*a^*b^*$ colour space used for colorimetric analysis. Adapted with permission from ref. 56. Copyright 2016 Institute of Food Technologists. (b) Variations of a^* , b^* colour coordinates during coloured to bleached switching of seven conjugated electrochromic polymers, (c) L^* values of a black electrochromic polymer in its neutral and bleached (oxidised) states. Reprinted with permission from ref. 52. Copyright 2011 American Chemical Society.

occasionally expressed in terms of a contrast ratio (CR) as illustrated below:

$$CR = \left(\frac{T_b}{T_c}\right) \text{ or } \left(\frac{R_0}{R_x}\right) \quad (2)$$

where T_b = intensity of light transmitted in the bleached state, T_c = transmittance in the coloured state, R_0 = reflected light intensity in the bleached state (or a reference white substrate), R_x = reflectance in the coloured state.

The above parameters are useful when describing the contrast at a single wavelength, either at the wavelength of maximum absorbance change (λ_{\max}) or at the wavelength of maximum human visual sensitivity (555 nm). On the other hand, when characterising a material that absorbs over a wide range of wavelengths (e.g. black to transmissive ECDs), it is more appropriate to report a change in luminance ($\Delta\%Y$) covering the whole visible spectrum. Luminance (cd m^{-2}) is a summation of all light transmitted, reflected and emitted in a given direction. Relative luminance, which is the normalised luminous flux density with respect to the illumination source, gives a better representation of the visually perceived colour changes of an EC display. In the smart-window industry, optical light modulations are mainly represented in terms of photopic contrast ($\Delta T_{\text{photopic}}$) between the tinted and bleached states.⁶⁰ Photopic transmittance represents transmittance over the visible region (380 nm to 780 nm) weighted to the sensitivity of the human eye and is defined according to the following equation:⁶¹

$$T_{\text{photopic}} = \frac{\int_{\lambda_{\min}}^{\lambda_{\max}} T(\lambda)S(\lambda)P(\lambda)d\lambda}{\int_{\lambda_{\min}}^{\lambda_{\max}} S(\lambda)P(\lambda)d\lambda} \quad (3)$$

where $T(\lambda)$ is the spectral transmittance of the device, $S(\lambda)$ the normalised spectral emittance of the light source and $P(\lambda)$ the normalised spectral response of the eye. When comparing performance of electrochromic materials and devices, it is therefore important to distinguish between the different approaches used to report optical contrast.

Apart from the wavelength of measurement, optical contrast depend on the thickness of the electrochromic layer^{39,62,63} as well as its morphology⁶⁴ and processing conditions.^{65,66} As the film thickness is increased, the transmittance of both the coloured and bleached states decrease usually in a non-linear manner, and the maximum contrast (ΔT_{\max}) is attained at an intermediate thickness (Fig. 4). Although the maximum transmittance change is generally determined on a trial-and-error basis, several models have been proposed to predict the ideal thickness,^{39,62} based on experimentally derived parameters, such as the linear correlation of absorbance with film thickness or redox capacity. It has been noted that a high volumetric redox density (number of redox sites available per unit volume) can be related to a high optical contrast for a given material.⁶⁵ Along with this notion, there is a general consensus that more porous structures facilitate better contrasts owing to the accessibility of a greater number of redox sites.^{64,67}

In general, high optical contrasts are desirable, however the scope of expected performance is dependent on the field of application.

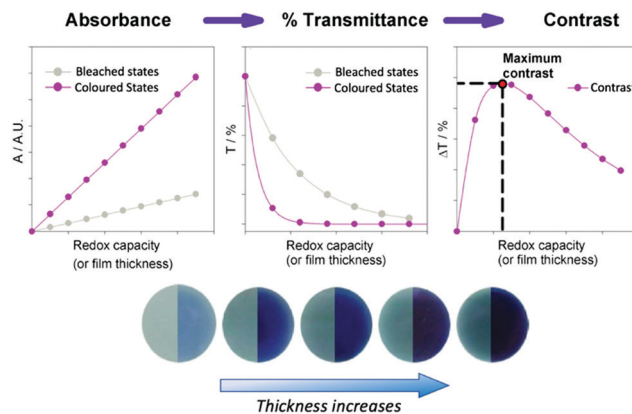


Fig. 4 Dependence of optical contrast on film thickness of PEDOT films. Figures reprinted with permission from ref. 65 (Copyright 2005 Elsevier) and ref. 62 (Copyright 2005 Elsevier).

For example, electrochromic windows and eyewear generally require photopic contrast to be greater than 60% (T_{photopic} in the range of 0.7 to 0.1 in the bleached and coloured states, respectively).^{22,68} High contrast values have been reported using various electrochromic materials, with metal oxides, conjugated polymers and plasmonics being at the forefront. Metal oxides show optical contrasts ($\Delta\%T$) typically around 50% (at 550 nm)⁶⁹ with nearly ideal contrasts reported using porous tungsten trioxide films (97.7% at 633 nm).⁶⁴ Conjugated polymers can also be engineered to show high optical modulations, especially those based on propylenedioxythiophene monomer derivatives (60–80%).⁶⁷ Plasmonics can be combined with commonly used electrochromic materials to increase their contrast by enhancing light interactions.⁷⁰ This strategy enables better contrasts to be achieved from thinner EC layers, thereby not compromising switching time in the effort to improve contrast.

3.5 Colouration efficiency

Colouration efficiency (CE) is a representative parameter of electrochromic performance, as it accounts for the charge requirement of electrochromic switching. It is defined as the optical change caused by a unit charge density (charge per unit area), usually measured at the wavelength of maximum absorbance, λ_{\max} .

$$CE(\eta) = \frac{\Delta OD}{Q(C \text{ cm}^{-2})} \quad (4)$$

Where ΔOD = change in optical density (measured in the form of either absorbance or transmittance), Q = charge injected or extracted per unit area of the electrochromic film.

Colouration efficiency is an intrinsic parameter of a material, and eqn (4) suggests that a value for CE can be obtained by the slope of a plot of absorbance change vs. charge density. However, for commonly studied electrochromic materials, including transition metal oxides and conjugated polymers, neither the optical density nor the charge density varies linearly over time when a constant potential (causing the oxidation or reduction of the material) is applied (Fig. 5a).⁷¹ Hence a plot of

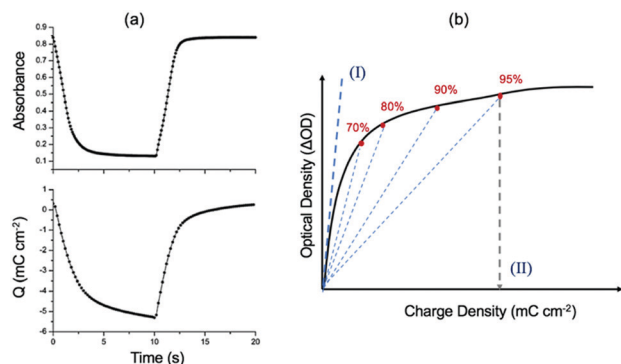


Fig. 5 (a) Non-linear variation of absorbance and charge density of a Prussian blue film coated on ITO measured by chronoabsorptometry and chronocoulometry when switched between +0.5 V and -0.2 V vs. Ag/AgCl reference in 0.2 M KCl. Adapted with permission from ref. 71. Copyright 2005 Royal Society of Chemistry. (b) General scheme representing a plot of ΔOD vs. charge density, with (I) and (II) representing commonly used approaches to calculate colouration efficiency.

ΔOD vs. Q also does not remain linear over the complete colour changing process. Therefore, the reported colouration efficiency will depend on the selected percent change of transmittance used for the calculation (Fig. 5b).

An approach using the linear portion of the ΔOD vs. Q graph as shown in Fig. 5b(I), is commonly employed to report the efficiencies of electrochromic transition metal oxides. However, this could lead to an overestimation, as it only accounts for the initial phase of colour change, but does not provide an accurate depiction of the overall switching process. In an effort to address this issue, the Reynolds group proposed measurement of a “composite colouration efficiency” (CCE), which calculates the charge required to attain a representative percentage (*e.g.* 95%) of the total transmittance change (ΔT), expressed in terms of:

$$\text{CCE} = \log \left(\frac{\%T_{0.95\Delta T}}{\%T_{\text{initial}}} \right) / Q \quad (5)$$

at the wavelength of maximum absorbance of the electrochromic material (Fig. 5b(II)).⁷¹ The remaining percent colour change (5%) that takes place much slowly should not contribute to a significant visually perceptible difference. In contrast, if the colouration efficiency calculation was to encompass the complete (100%) switch, it would be misleading as it indicates an underestimated performance than what is observed in an actual device.⁶⁷

Another important factor adding to the complexity of the colouration efficiency calculation is the distinction between faradaic and non-faradaic currents that contribute towards the net current. Owing to the parallel, layered-like structure of the electrochromic device, a capacitive current is inherently present. In principle, however, it is only the faradaic current that controls the colour change of redox-based electrochromic materials. Calculation of the colouration efficiency based on the net current will result in an underestimated CE values, while delineating electrochemical processes that are directly involved in the colour change would reveal more meaningful details for the comparison of materials.⁷²

There are continuing efforts to design materials which undergo large absorbance changes with minimal charge, that can be interfaced with low-power energy sources. Devices incorporating amorphous WO_3 have shown colouration efficiencies between 40–60 $\text{cm}^2 \text{C}^{-1}$, with variations arising from different morphologies and selected wavelengths.⁶⁹ In general, organic electrochromic materials have higher CE values compared to the traditionally used inorganic EC materials.⁶⁷ For example, electrochromic dyes and viologens have CEs in the range of 150–600 $\text{cm}^2 \text{C}^{-1}$ and conjugated polymers exhibit CEs close to 100–800 $\text{cm}^2 \text{C}^{-1}$. Devices made from polymer-based electrochromic and counter electrodes can operate at very high efficiencies ($> 1000 \text{ cm}^2 \text{C}^{-1}$).⁷³

In summary, colouration efficiency determines the relative ease with which the colour is modulated *via* the application of an external bias. When using this parameter to evaluate the EC performance, appropriate optical contrast measurements should be made to reflect the applicability of the material. The intrinsic redox activity of the material, the doping level, applied potential,⁷⁴ film deposition process⁶⁹ and electrolyte interactions also influence this parameter.

3.6 Switching time

The time required to switch between different electrochromic states, also known as the response time, is a key parameter when considering the suitability of an electrochromic device for applications. Similar to the parameters described above, switching time is also interpreted in different ways and the non-specificity of the reported data makes it challenging to meaningfully compare between materials, fabrication techniques and device designs. The generally accepted method is to report the time taken for a required percentage (*e.g.* 90%) of the complete optical switch to occur, when square-wave potential pulses are applied on the working electrode (Fig. 6a and b). Again, the optical contrast can be measured as an absorbance or transmittance change at λ_{max} , wavelength of maximum sensitivity (555 nm), or as photopic contrast, as described in Section 3.4. The alternative approach is to track the current evolution when the switching potential is applied, and to record the time taken for the current flow to change by a specified percentage during the chronoamperometric measurement (Fig. 6c).^{75–77}

A recent study highlighted the importance of standardising the method in which switching time is reported.⁷⁸ This employs application of square wave potentials of different pulse lengths to the electrochromic material, and fitting the transmittance changes corresponding to these pulses to an exponential increase function to obtain a time constant (τ) that is representative of the switching kinetics of the material with respect to its maximum attainable contrast (Fig. 6d–f). The time constant τ , measured in seconds, corresponds to the time taken for the material or device to undergo $\approx 63\%$ of its maximum optical contrast ($\Delta T(\%)_{\text{max}}$), with 2.3τ and 3τ representing 90% and 95% of $\Delta T(\%)_{\text{max}}$.

The above parameter provides an averaged switching time for the colouration and bleaching processes, enabling a direct

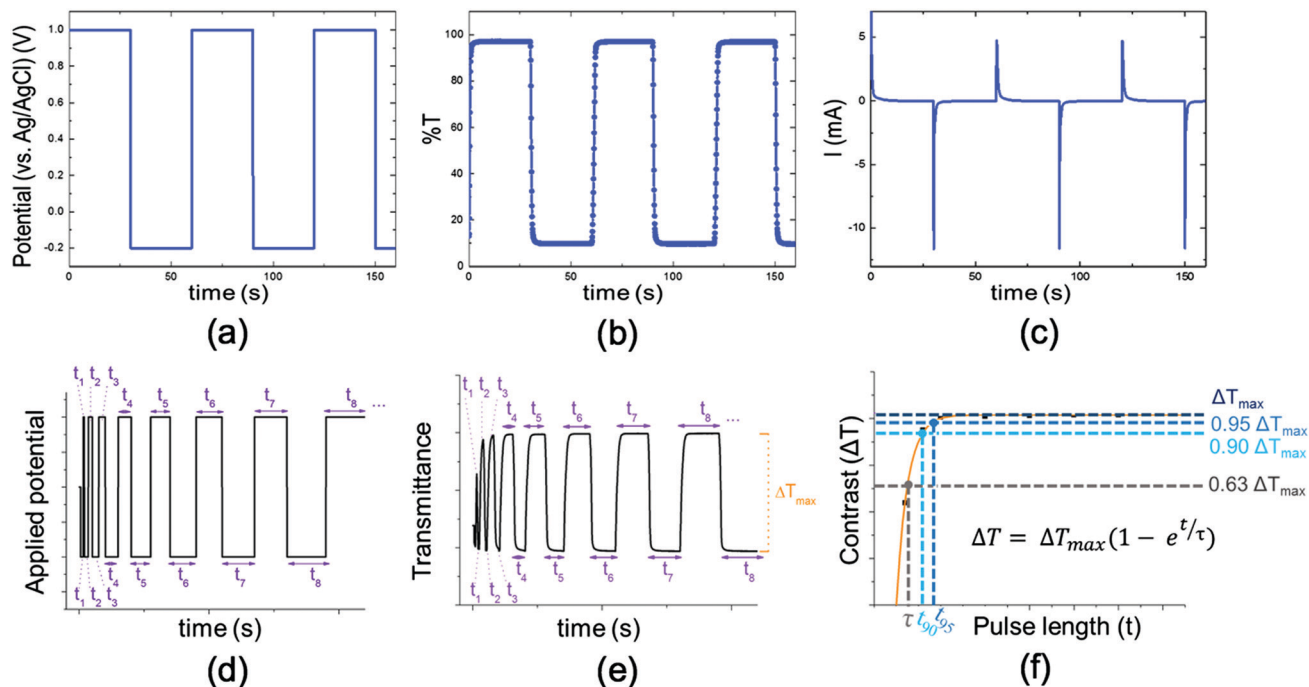


Fig. 6 Measurement of switching time. (a) Square-wave potentials (V_1 and V_2) applied in a chronoamperometric experiment, (b) variation of transmittance and (c) current response during switching. (d) New standardised approach for reporting switching kinetics of an electrochromic material by application of symmetric potential pulses of different lengths and (e) simultaneous transmittance measurements, followed by (f) data fitting to an exponential function to obtain the time constant τ . Adapted with permission from ref. 78. Copyright 2018 Elsevier.

comparison of the switching kinetics of electrochromic devices. However, the switching times for forward and reverse reactions (switching back and forth) may be different due to the different mechanisms involved in the process, with significant differences arising for slow switching materials. The aforementioned technique can then be adjusted accordingly to reflect these changes. Apart from intrinsic parameters such as colouration efficiency, film thickness and morphology, extrinsic factors including electrolyte type, ionic diffusion coefficients, counter electrode and substrate sheet resistance, device geometry and size, can all influence the switching kinetics of an ECD.^{78,79}

3.7 Cycling stability

The long-term cycling stability of electrochromic materials can be evaluated by observing the loss of the optical contrast and charge density upon repetitive electrochemical cycling. Materials capable of maintaining over 95% of its maximum optical contrast during the application of boundary potentials in the form of square-wave pulses, are deemed stable.^{80,81} The loss of the charge or peak current density is also used to evaluate the stability of the electrochromic materials when they are subjected to repetitive cyclic voltammetry tests.⁸² Stable electrochromic materials are expected to exhibit cycle life of more than 10^4 cycles depending on the applications. In the application of the building windows, if the ECDs go through a complete on/off cycle minimally twice a day, then at least 15 000 cycles will be required for the materials to maintain a stability over 20 years. Nevertheless, ECDs used in

eyewear and rear-view mirrors will be switched more frequently and thus 10^6 cycles are required. In the laboratory exploration of new materials, the stability of the electrochromic materials is often reported using only the loss of the optical contrast with the light focused on a particular area of the electrochromic film, while the failure could happen outside of this focus point. To provide a complete picture, the cyclic voltammograms before and after the cycling test should be provided together, so that the condition of the overall thin film can be evaluated.³³ Moreover, the cycling stability results obtained from the platinum electrode do not necessarily reflect the stability on the ITO or FTO transparent electrodes that are used in most of the applications, since the adhesion of the electrochromic materials on different substrates might be very different.^{83–85}

3.8 Application-specific performance metrics

Apart from the standard performance parameters mentioned above, additional characteristics related to specific applications of electrochromic devices are also worth considering. The following section will mainly focus on the performance indicators used to evaluate stable electrochromic windows and their practicality from the perspectives of energy consumption and environmental stability.⁸⁶ Windows are exposed directly to solar radiation, encompassing wavelengths in the UV, visible and near-infrared regions (300–2500 nm),⁸⁷ and electrochromics offer a method by which both light and heat transmittance can be modulated. As described in Section 3.4 eqn (3), the photopic transmittance (transmittance in the visible range, T_{photopic}) is

used to represent the extent of visible light that is transmitted through the window, in its bleached and tinted forms. However, to evaluate the complete energy response, it is necessary to consider parameters pertaining not only to visible light but also to thermal energy.

3.9 Colour rendering index (CRI)

A switchable window glazing can alter the spectral profile of a light source as the light passes through the device.⁸⁸ Especially when blocking natural daylight using the coloured (tinted) state of the EC window, the spectral characteristics of the coloured state can significantly impact the colour rendering of interior objects. For example, if the tinted glass corresponds to dark blue or brown, the colours and brightness of objects viewed from the interior of the building would appear much different to what's usually observed under natural daylight (spectral shift). The colour rendering index (CRI) is a quantitative measurement of the colour appearance of an object illuminated by an unnatural light source compared to its colour with an ideal or natural light source.⁷⁹ The method of calculation is outlined by CIE,⁸⁹ where a value of 100 implies perfect colour matching. As the transmittance in the visible range decreases, the colour rendering mismatch increases. In terms of lower colour attenuation, neutral grey glazing is preferred over blue or brown.⁷⁹ It has been reported that a single CRI value is unable to accurately describe the extent of colour desaturation caused by external glazing,^{88,90} and a two-measurement method, IES TM-30-15,⁹¹ measuring both the colour fidelity and colour gamut (saturation or vividness),⁹⁰ or colour differences (ΔE , as described previously)⁸⁸ would be more representative.

3.10 Solar heat gain coefficient (SHGC) and thermal transmittance

Smart windows have the potential of minimizing energy consumption for temperature regulation by controlling heat gain or loss (cooling and insulation) through windows as desired, and are therefore considered key components in energy-efficient, green building technology.⁹² Solar irradiance incident on a window is mainly transmitted, absorbed and reflected. The absorbed solar energy can also be transmitted inwards through processes of conduction, convection and radiation⁸⁷ (Fig. 7a). As such, the total energy transmitted through an electrochromic window is quantified by a parameter known as the solar heat gain coefficient (SHGC) that represents the solar radiation entering a building as a fraction of the total incident radiation. It is calculated either by simulations⁹³ or by measuring the total heat flow using a calorimeter chamber.⁹⁴ SHGC values of 0.6 and 0.2 are usually recommended for winter and summer as a general guideline.⁸⁶ For example, according to the American Society of Heating, Refrigerating and Air-Conditioning Engineers (ASHRAE) 90.1 2007 national energy code, static glass SHGC values of 0.25 and 0.4 are recommended for Arizona and Minnesota, respectively.⁹² Electrochromic materials that can bring about this change would be highly desired. Solar heat gain alteration using electrochromic glazing as shown in Fig. 7b aids the heating or cooling process of the building in response to the climate.

Electrochromic polymers can be used to selectively block either the IR-radiation, or visible light, or in certain cases, the UV radiation (described further in the materials section). When compared to traditional, single-component inorganic electrochromic materials,

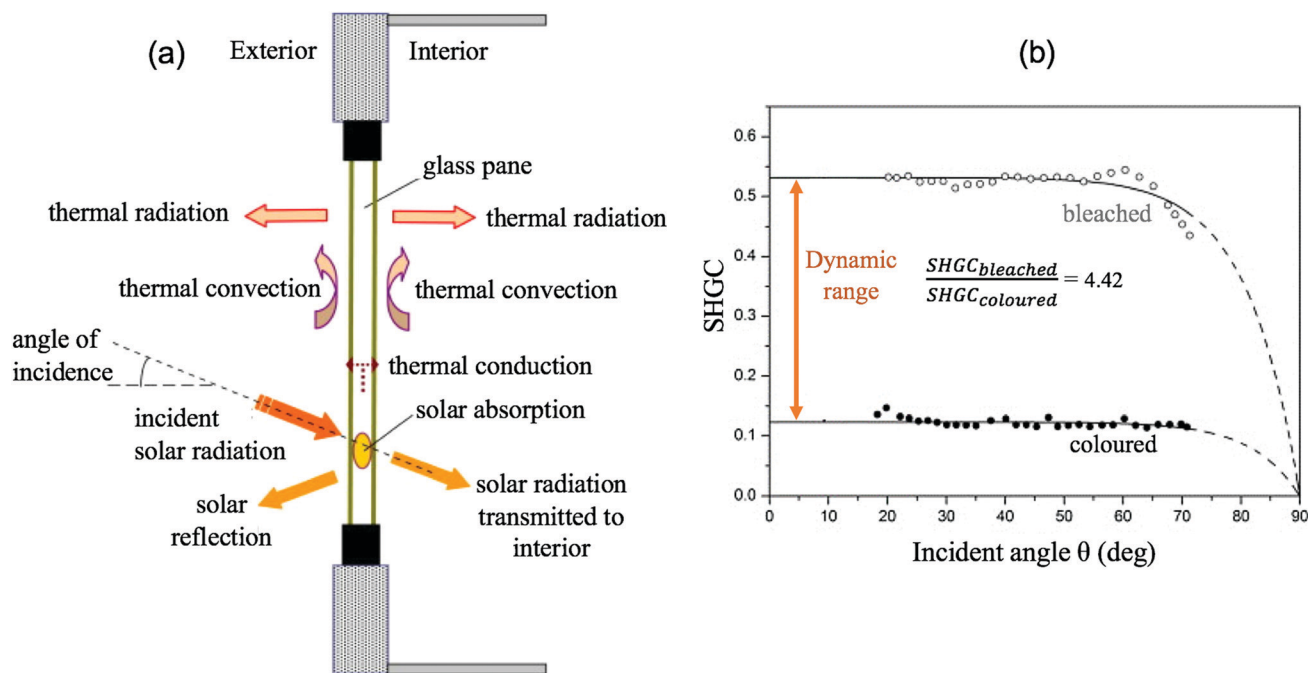


Fig. 7 (a) Modes of solar energy transfer through an electrochromic window. Adapted with permission from ref. 87. Copyright 2009 Elsevier. (b) Angle-dependent SHGC changes in the coloured and bleached states of an electrochromic window using WO_3 and NiO as electrochromic and counter electrodes, respectively. Reprinted with permission from ref. 86. Copyright 2015 Elsevier.

NIR-modulating nanostructured electrochromic materials^{32,95} (nanocrystalline indium-doped tin oxide,³¹ aluminium-doped zinc oxide⁹⁶ and WO₃ nanowires⁹⁷) can be beneficial in obtaining enhanced thermal control, without compromising the visible light transmittance.

A building can also lose heat through its windows, and alternative products with lower thermal transmittance are sought for better thermal insulation in colder climates. Thermal energy loss through a material or device can be calculated using the thermal transmittance coefficient (U). It quantifies the rate of total heat flow (conductive, convective and radiative) stemming from a temperature gradient across the window, and is expressed in terms of $\text{W m}^{-2} \text{K}^{-1}$ (or in $\text{Btu h}^{-1} \text{ft}^{-2} \text{°F}^{-1}$).⁸⁶ The electrochromic layer should meet standard thermal insulation requirements. U -Values typically less than $1.2 \text{ W m}^{-2} \text{K}^{-1}$, or lower ($0.57 \text{ W m}^{-2} \text{K}^{-1}$)⁹⁸ are recommended for regions with warmer climates. Additionally, heat losses can be further reduced by utilising device architectures with multiple glass panes filled with transparent, low-conductivity gases or vacuum, which are coupled with anti-reflective coatings and low-emissivity (low-e) coatings such as FTO (fluorine-doped tin oxide).⁸⁶ U -Value calculation and SHGC calculation based on the U -value can be described as follows.⁹⁹

$$U = \left[\frac{1}{h_o} + \frac{1}{h_i} + \frac{L}{k_t} \right]^{-1} \quad (6)$$

$$\text{SHGC} = T_{\text{solar}} + \frac{A_{\text{solar}} U}{h_o} \quad (7)$$

Where h_o and h_i are the thermal conductivities of the outer and inner surfaces of the window, k_t is the thermal conductivity of the window material, L being the thickness of the window, and A_{solar} and T_{solar} representing the absorbance and transmittance of solar radiation by the EC window.

4. Electrochromic materials

Over the past decades, the field of electrochromic materials has evolved to encompass different classes of materials, including transition metal oxides, small organic molecules, metal-organic complexes, conjugated polymers and plasmonic materials. Several review articles have covered these electrochromic materials.^{12,100–107} The focus of this section is to provide a brief overview of the transition metal oxide, plasmonic, and polymer based electrochromic materials, their working mechanisms, performance, stability, and their processing compatibilities with large-scale roll-to-roll techniques.

4.1 Transition metal oxides

Electrochromic transition metal oxides exhibit tuneable colour change in the visible and infrared region under external potentials, arising from simultaneous electron (from conductive substrate) and cation (from electrolyte) injection or extraction during the electrochromic processes.¹⁰¹ Most commonly reported electrochromic transition metal oxide structures that are both electron and ion conductive are composed of highly

distorted MO₆ octahedra,^{108,109} with M denoting the transition metal. The edge- or corner-shared octahedra form layered-like structures, leaving atomic openings for the intercalation of proton or alkali ion species. Main categories of electrochromic transition metal oxides can be classified by their trends of colour change under external potential: transition metal oxides that are coloured by cathodic potentials are noted as cathodically colouring electrochromic materials (coloured in the ion-intercalated state), as electrons injected to the materials are balanced by ion intercalation, leading to the colouration processes.¹¹⁰ Anodically and intermediate colouring materials are also widely reported and utilised, and will be introduced later in the counter electrode section.¹¹¹

Tungsten trioxide (WO₃) is one of the most extensively studied cathodically colouring electrochromic transition metal oxide, changing from a bleached state to a coloured state under cathodic (reducing) potentials.⁶⁹ Pristine, bulk WO₃ exhibits native oxygen deficiencies,¹¹² giving rise to a light yellow/green colour as compared to white colour of stoichiometric WO₃, and becomes blue upon application of a reducing potential.¹¹³ The colouration mechanisms have been predominantly described as (intervalence) charge transfer and small polaronic absorption.^{7,114–118} Additional consideration, especially the effect of composition, defect type and density, oxygen vacancies and crystallinity, need to be accounted to illustrate the colouring mechanisms.^{119–123} However, despite the variance in synthetic parameters and sample qualities, the electrochemically triggered colour change in WO₃ is typically described as WO₃ (bleached) + $x\text{e}^- + x\text{H}^+ \rightleftharpoons \text{H}_x\text{WO}_3$ (coloured), where H^+ can be substituted by alkali cations, indicating the colouration process is accompanied by the uptake of an electron balanced by proton or alkali ion intercalation.¹¹¹

The understanding of the electrochromic performances of WO₃ helps rationalizing the structure–property relationship of electrochromic transition metal oxide materials extending to many other compositions and structures. In particular, crystallographic and morphological structures impact the electrochromic switching time, optical contrast and cycling stability. For example, nanoscale WO₃ structures, including nanoparticles,¹²⁴ nanorods,¹²⁵ nanosheets,¹²⁶ hierarchical meso/microporous structures,¹²⁷ and anodised particle films¹²⁸ are typically reported to exhibit shorter switching time, larger colouration efficiencies, and higher cycling stabilities than their bulk counterparts, as they have higher interfacial contact area with the electrolyte, shorter diffusion path lengths and feasible strain relaxation and phase transformation associated with the intercalation and de-intercalation processes (Fig. 8), giving rise to their highly efficient and stable performances. Amorphous WO₃ films typically exhibit higher coloration efficiencies (on the order of $10^2 \text{ cm}^2 \text{C}^{-1}$) than their crystalline counterparts, although dissolution of the amorphous WO₃ structures in proton and Li ion based electrolytes remain a challenging issue.^{124,129–131} Hierarchical nanocrystal-in-glass tungsten oxide thin films, where crystalline WO₃ nanoparticles are embedded in amorphous WO₃ matrix, encompass the advantage of both attributes, leading to enhanced

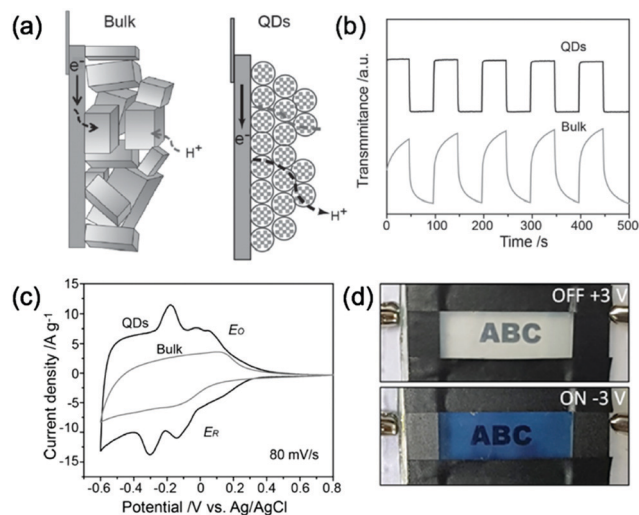


Fig. 8 (a–c) Improved switching kinetics (within 1 s) of WO_3 QDs. Adapted with permission from ref. 133. Copyright 2014 John Wiley and Sons. (d) Bleached (top) and coloured (bottom) state of two dimensional WO_3 nanosheets. Reprinted with permission from ref. 126. Copyright 2018 American Chemical Society.

electrochromic properties.¹³² The structural and morphological design principles for electrochromic WO_3 share many parallels with transition metal oxide based ion storage materials for counter electrode, which will be discussed in the next section.

Because the electrochromic properties of transition metal oxides can be affected by their size,¹³³ porosity¹³⁴ and crystallinity,¹²³ the processing techniques and conditions need to be well-controlled to achieve reproducible performances. Synthetic and fabrication techniques like electrodeposition¹²⁸ and evaporation methods¹³⁵ typically produce amorphous films, while sputtering¹³⁶ may induce partial crystallinity depending on the deposition parameters. Commercialised electrochromic device manufacturing processes employ magnetron sputtering on glass or on PET substrates for “retrofitting” existing glass windows with flexible PET substrates.¹³⁷ With this method, sequential deposition of metal oxide films as the working and counter electrodes exhibiting stable device performances have been developed. A proposed mechanism for a streamlined sputtering process and device lamination is shown in Fig. 9(a).

4.2 Doped plasmonic oxide materials

Conventional metal-based plasmonic nanostructures exhibit intrinsic free carrier densities on the order of 10^{22} cm^{-3} ,¹³⁸ which give rise to enhanced localised surface plasmon resonance (LSPR) near the surface of the particles.¹³⁹ Some metal-based plasmonic nanostructures like Ag particles have been used as electrochromic active materials, as Ag^+ undergo reversible deposition (to Ag^0 , coloured) and dissolution (to Ag^+ , colourless) under external bias.^{140–142} Similarly, dynamic windows based on reversible electrodeposition of Cu–Pb, Cu–Ag¹⁴³ and Bi/Cu¹⁴⁴ composite materials have been demonstrated, exhibiting good optical contrast and durability. While the specific colour of the

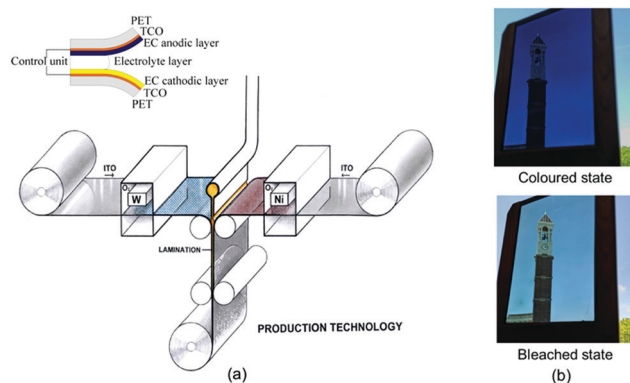


Fig. 9 (a) Schematic of streamlined ECD manufacturing with metal oxide sputtered on PET substrates. Inset: Proposed layered ECD fabricated using the streamlined process. Adapted with permission from ref. 137. Copyright 2017 Elsevier. (b) View through an electrochromic window in the coloured and bleached states.

ECDs utilising conventional plasmonic nanostructures can be tuned by the size and shape of the nanostructures,^{141,142} doped metal oxide based plasmonic nanostructures allow for more degrees of freedom in spectral selectivity, because of their dynamically tuneable free carrier densities, which can be synthetically and post-synthetically controlled, without involving the size and morphology changes of the nanostructures.¹³⁸

Degenerately doped metal oxide nanoparticles exhibiting localised surface plasmon resonance (LSPR) properties allow electrons to be accumulated within or depleted from the plasmonic metal oxide nanoparticles under applied voltage.¹³⁸ Shown in Fig. 10, electrochemically controlled injection or extraction of the electrons, along with attraction or repulsion of counterions at the electrode–electrolyte interface, are induced by the application of negative and positive potentials. Such capacitive charging processes lead to varying free carrier concentrations, thereby achieving changes in LSPR peak position and intensity, and tuneable colour changes in the visible and near infrared region.¹⁰³

A large body of work has been demonstrated on the prototypical $\text{Sn:In}_2\text{O}_3$ (ITO) and Al:ZnO (AZO) nanoparticle systems, where plasmonic resonance frequencies can be synthetically tuned by varying the particle sizes and doping ratio during the synthesis, and modulated post-synthetically by dynamic charge injection *via* external voltage.^{31,96,145,146} For the application of

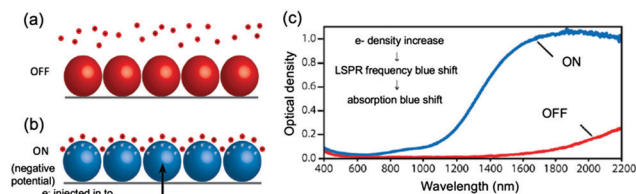


Fig. 10 Schematic representation of electrically modulated LSPR doped metal oxide nanoparticles and corresponding spectroscopic responses. Figures a–c are reprinted with permission from ref. 32. Copyright 2014 Royal Society of Chemistry.

LSPR oxides and exploration of new LSPR metal oxide particles as electrochromic materials, it is particularly important to synthetically control the incorporation of dopant species into host metal oxide particles, which requires not only the balancing of precursor reactivities and dopant induced lattice strain,^{147,148} but also the identification and understanding of the nature and distribution of dopant species.^{149–152} For ensemble LSPR metal oxide particles in the form of thin films, the homogeneity and monodispersity of the particle sizes, morphologies, dopant concentration and distribution are all important factors that impact the LSPR properties.¹³⁸ In addition, ligand exchange, film thickness, porosity and inter-particle coupling impact the LSPR properties of assembled particle films,^{31,153–156} and design of “particle-in-matrix” composite can potentially enhance the spectral selectivity of the composite electrochromic materials.^{157–159}

The solution processability of the aforementioned plasmonic metal oxide materials typically relies on their surface ligands. As the plasmonic nanostructures are generally monodisperse particles within the size range of tens of nanometres, their surfaces are capped with long hydrocarbon ligands that give rise to good dispersibility in non-polar solvents, but form insulating barriers and prohibit charge transfer in electrochromic devices. Removal of the surface ligands have primarily been demonstrated *via* ligand stripping^{96,152,160} and thermal annealing^{149,161} after the coating of plasmonic particle thin films. Film volume change and chemical compatibility issues need to be considered during the ligand stripping processes,¹⁶² and annealing methods often require stringent control of processing conditions to avoid alteration of the optical properties of the particles.^{149,161} Looking forward, expanding the library of synthetic and post-synthetic methods for removing or substituting the long hydrocarbon ligands will benefit the large scale applications of plasmonic nanostructures in electrochromic devices.

4.3 Electrochromic polymers

Semiconducting polymers have rendered themselves useful in display technology (OLEDs), photovoltaics (organic solar cells), transistors (OFETs) and charge storage devices (batteries, supercapacitors), which benefit from the lightweight, flexible nature of the polymers as well as their compatibility with large-area, low-cost fabrication methods.^{163–167} Such advantages of polymers hold true for ECDs as well, but they also bring a host of added advantages unique to electrochromics, including improved switching kinetics, better contrasts and lower power consumption when compared with the previously mentioned electrochromic transition metal oxides.^{168–171} Paired together with the advanced synthetic versatility of organic chemistry, ECPs enable guided design of material properties such as colour, redox activity, solvent compatibility, and processability along with polymer mechanical properties that relate to film porosity, morphology and degree of crystallinity.¹⁷²

Mechanism of colour change. Most EC polymers are highly conjugated (containing alternating double and single bonds), usually comprising of heterocycles along its backbone. The high degree of π -orbital overlap creates a band-like electronic

structure, with the Highest Occupied Molecular Orbital (HOMO) residing in the valence band and the Lowest Occupied Molecular Orbital (LUMO) in the conduction band. Electronic transitions from the HOMO to the LUMO (π - π^* transitions) determine the onset of a polymer's absorption spectrum, and transitions pertaining to wavelengths in the visible region (380–780 nm *i.e.*, 1.8 to 3.1 eV) are responsible for the colourful appearance of most conjugated polymers. The mechanism leading to their colour change is closely related to that of metal oxides and involves oxidation (p-doping) or reduction (n-doping) of the neutral polymer. In an electrochemical cell these redox processes occur in conjunction with counter-ion diffusion into the polymer layer to maintain electroneutrality.¹⁷³ Based on this dual transport of ions and electrons, these materials are also commonly referred to as mixed-ionic electronic conductors.¹⁷⁴ The doping process induces changes in the electronic structure and lowers the HOMO–LUMO energy gap when transitioning from the neutral polymer to a singly charged (polaron) radical state, and subsequently to a doubly charged state (bipolaron).^{175–177} The long conjugation and π - π interactions of the polymers facilitate charge distribution in the doped state, favouring the formation of the bipolaron, hence enabling a switch in the spectral absorption into longer wavelengths, as observed by spectroelectrochemical measurements; represented below in Fig. 11. These bandgap alterations resulting from polymer doping can either cause spectral shifts within the visible range (*e.g.* colour changes from red to blue) or be significantly large to shift the absorption profile from the visible region to the near IR (or from UV to the visible region).^{49,178,179} Polymers that switch between coloured and transmissive states are commonly classified as cathodically colouring (coloured by reduction) or anodically colouring (coloured by oxidation).¹⁸⁰ These terms are not to be confused with “anode-active” (p-type) and “cathode-active” (n-type) polymers that refer to the intrinsic redox activity of the polymer.

Colour tuning of ECPs. When ECDs are designed for display and window applications, it is important to design aesthetically appealing colour combinations. Conjugated polymers have a significant advantage in terms of colour tunability when compared to the widely used transition metal oxides. Although the band gap mainly dictates the absorption onset, the perceived colour of a π -conjugated material is a result of the combinative input of all optical transitions present across the spectrum taken together with their relative intensities. Intermolecular interactions including vibronic transitions, charge-transfers and aggregation features can significantly influence the colour of a polymer.¹⁸¹

Colour tuning of electrochromic polymers (ECPs) have been extensively studied, especially for those that are cathodically colouring, switching from a coloured to a bleached state upon oxidation. Two approaches have been mainly used: (1) spectral engineering through structural modifications to tune the absorptive properties and (2) blending of electrochromes to generate new colours by superposition of absorptive features guided by the subtractive colour mixing theory. Some excellent reviews on both strategies have been published over the past years,

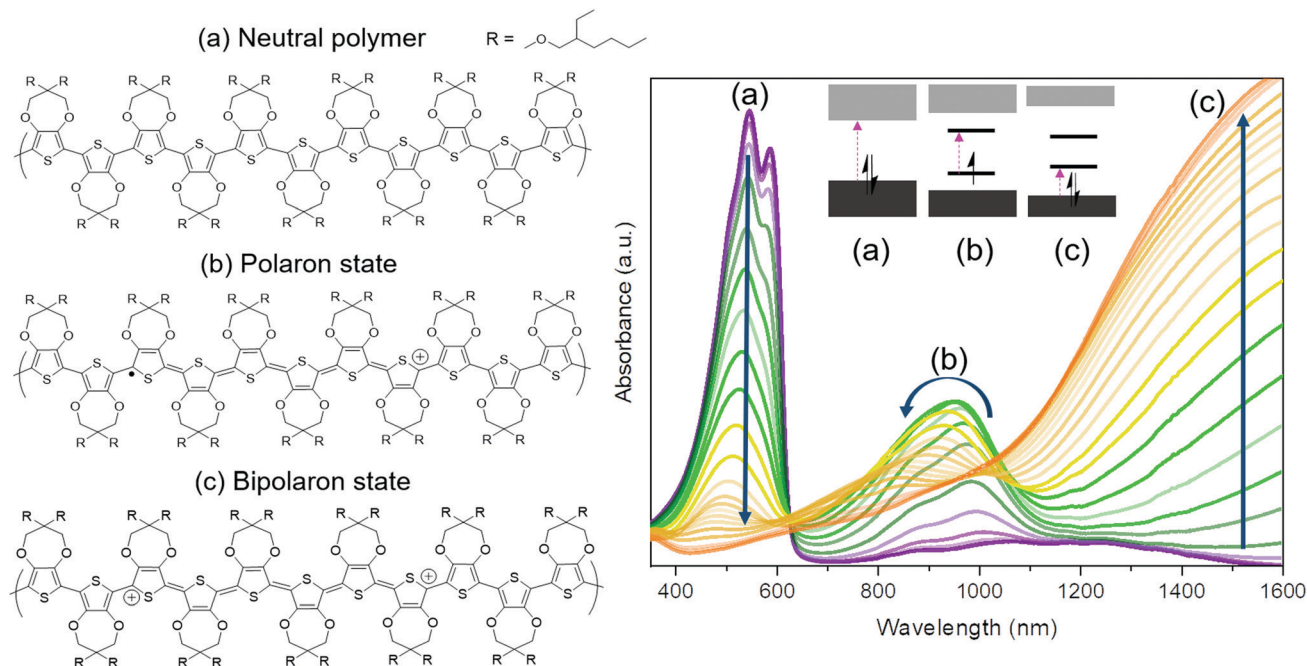


Fig. 11 Spectral changes occurring in a cathodically-colouring polymer (ECP-magenta) tracked by spectroelectrochemistry (potential range 0.0 to +1.0 V). Absorbance of the neutral polymer (a) in the visible region gradually shifts to the near IR range upon oxidation, forming the polaron (b), followed by the bipolaron (c).

delimiting methods for monomer design and polymerisation techniques to attain polymers of desired colours.^{10,11,52,59,181–188}

When looking into the toolbox available for colour control, some key factors can be clearly identified regarding the design of the polymer backbone and/or the side chains.^{10,189} The vast majority of reported ECPs stem from a few main building blocks, namely the thiophene, pyrrole, benzothiadiazole, fluorene, carbazole and phenylenevinylene units. To tune the bandgap of the pure polymers, the monomer can be altered by replacing the heteroatom of the structure, functionalising with substituents that enhance or deplete the electron density of the conjugated system, or be copolymerised with other conjugated systems in a random or statistical manner.^{190–195} It needs to be noted that these modifications not only affect the colour but can also have an impact on the redox potentials, optical contrast, switching kinetics and thin film processability.^{196–198}

The critical role of backbone substituents can be clearly understood by considering the classic example of designing polythiophene-based electrochromic polymers (Chart 1).

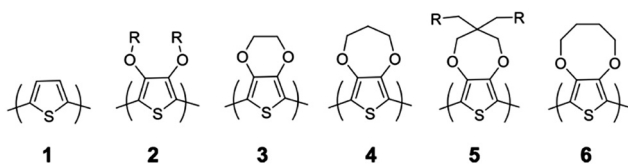


Chart 1 Chemical structures of thiophene-based electrochromic polymers. Polythiophene (1), 3,4-substituted polythiophene (2), polyethylenedioxythiophene (PEDOT) (3), poly(propylenedioxythiophene) (PProDOT) (4), alkyl-substituted PProDOT (5) and poly(butylenedioxythiophene) (PBuDOT) (6).

Polythiophene (1), which is usually deposited *via* electropolymerisation, has a bandgap of approximately 2 eV and shows a colour change from red to blue upon oxidation.¹⁸⁵ The absorption spectrum of polythiophene can be blue-shifted by substituting the 3 and 4 positions of the thiophene monomer with bulky substituents, such as ethylhexyloxy groups (2). The branched substituents induce sufficient torsional strain on the backbone to disrupt the conjugation, which makes the neutral polymer appear orange, while also improving its solution processability.¹⁹² Conversely, attaching an electron donating ethylenedioxy unit at the 3 and 4 positions of thiophene (PEDOT, 3) increases the electron density at the thiophene unit, lowering the oxidation potential and decreasing the band gap to 1.6 eV. Therefore, the absorption spectrum of PEDOT is red-shifted with respect to polythiophene. Neutral PEDOT, which is prepared through oxidative or electrochemical polymerisation techniques, is dark blue and switches to a transmissive light blue upon oxidation.^{184,199,200} Due to solubility limitations, PEDOT is frequently used in the form of a polyelectrolyte dispersion, together with the polystyrene sulfonate (PSS) anion. Several attempts have been made to improve solution-processability of PEDOT by attaching solubilizing groups such as long alkyl chains (C14) and charged groups such as sulfonates, or by copolymerizing with monomer units such as propylenedioxythiophene (ProDOT).^{198,201–203} In the case of ProDOT (4), the incorporation of an additional C atom onto the alkylene bridge (propylene instead of ethylene) enhances the non-planarity of the polymer backbone, inducing a slight blue-shift in the absorbance onset and improved optical contrast.¹⁹⁶ Additionally, ProDOT allows for tetrahedral substitution at the central

carbon (5) and the presence of bulky substituents orthogonal to the main chain causes further blue-shifting of the absorption spectrum (e.g. ethylhexyloxy substituted ECP-magenta), improve solution processability and favour the formation of more “open” or porous morphologies that facilitate counter ion transport through the film, leading to even higher optical contrasts, faster EC switching and better colouration efficiencies.^{204–209} If the size of the ring fused onto the thiophene monomer is made even larger, as in the case of poly(butylenedioxythiophene) (6), the switching time and optical contrast is enhanced further, owing to the favourable morphology of the polymer film allowing facile interaction with the electrolyte.¹⁹⁶ It needs to be noted that side-chain engineering for electrochromic polymers is much less stringent than for transistor or solar cell applications, as maintaining high conductivity is not a crucial factor.²¹⁰ These strategies taken together enable conjugated polymers to attain an improved electrochromic performance than metal oxides. Pioneering work developed by the Reynolds group demonstrated the rational design of anode-active cathodically colouring ECPs covering the entire colour palette,⁵² making use of the aforementioned strategies and the versatility of organic synthesis (Fig. 12).^{21,192,194,211–216}

Design of certain coloured polymers are more challenging than others. For example, many research efforts were dedicated in designing a green polymer, which required dual band absorption (absorption in the red and blue regions, leaving the green region transmissive).¹⁸¹ Donor-acceptor copolymer approach is now commonly established as a route for attaining such colourations, and also when synthesizing widely absorbing polymers, such as ECP-Black.^{216–219} A few examples

on anode-active, anodically colouring polymers are also available, mainly based on *N*-substituted (3,4-dioxypyrrroles), fluorenes and triarylamines.^{188,220–226} These polymers have much wider band gaps, absorbing in the UV region in their neutral state and switching to the visible region upon oxidation. Especially in the case of triarylamine-based polymers, the N atom acts as a conjugation breaker due to the non-planar conformation of the neighbouring phenyl rings, hindering the ready formation of the fully oxidised form. This makes the isolated radical cations accessible, and leads to the observation of differently coloured transition states depending on the number of triarylamine groups present in the repeating unit (Fig. 13).²²⁷ Not many n-type EC polymers have been reported as a result of the instability of the doped states in the presence of oxygen and moisture.

As described earlier, a key advantage of ECPs is the ease of processing. The main strategy for achieving solution processability

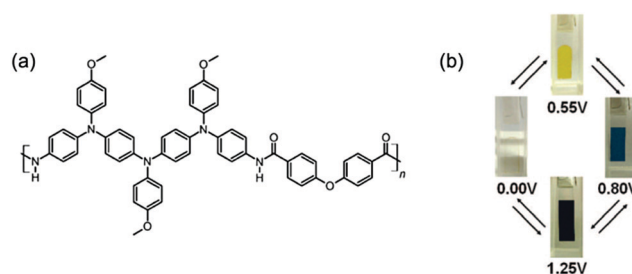


Fig. 13 (a) Chemical structure and (b) anodic colouration of triarylamine polymers. Figure (b) is reprinted with permission from ref. 227. Copyright 2008 American Chemical Society.

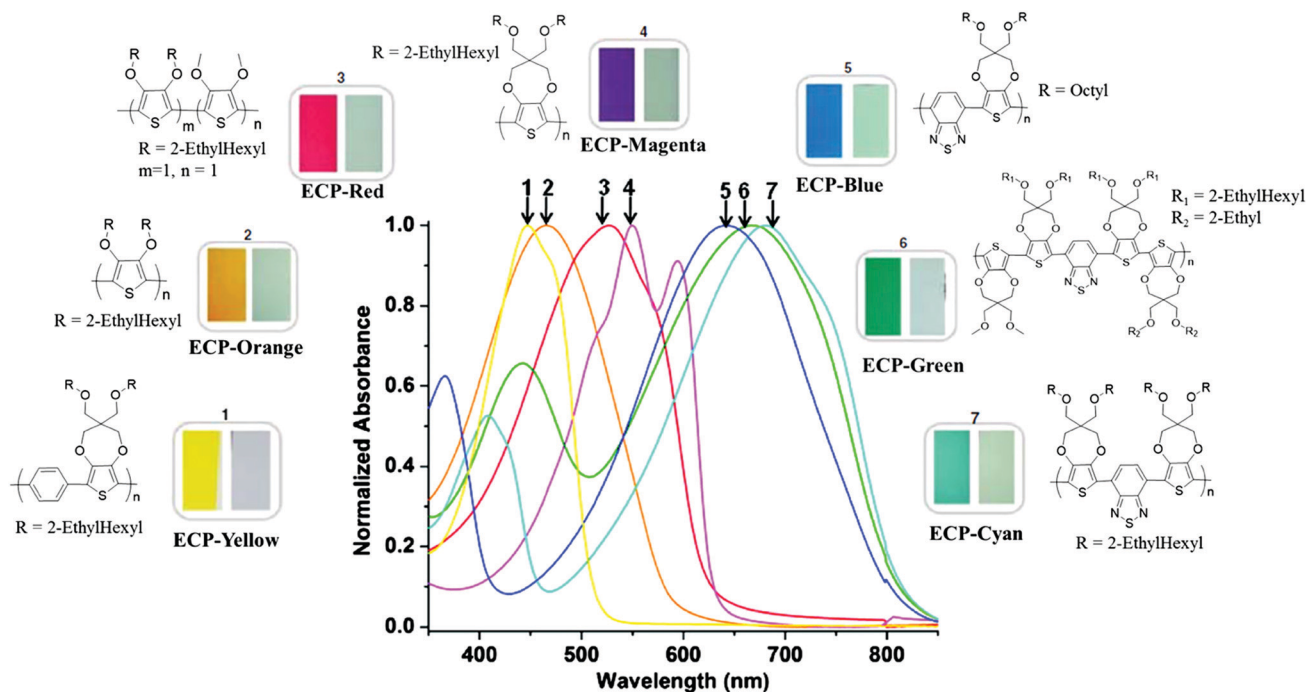


Fig. 12 Absorption spectra of cathodically-colouring conjugated polymers of different colours. Reprinted with permission from ref. 52. Copyright 2011 American Chemical Society.

is to reduce the inter-chain packing using linear or branched alkyl side chains.²¹⁰ Enhanced solubility in organic solvents enable thin films to be fabricated using fast and efficient processes such as spin-coating, blade coating, spray casting or drop-casting, instead of electrodeposition, which has intrinsic limitations in scale and productivity.^{52,194,202,208,228} Commonly employed solvents include dichlorobenzene, chlorobenzene and chloroform, because of their ability to form uniform thin films with favourable morphology. However, when considering scaled-up deposition, substitution of such halogenated solvents with environmentally-benign ones would be favourable, as large volumes of solution are continuously used up and evaporated in the drying process of a roll-to-roll printing setup. To this end, toluene and xylene are currently used in large-scale depositions, while the ultimate goal would be to achieve processability from green solvents such as esters, alcohols or water.^{229–232} The prototypical conducting polymer, PEDOT:PSS, is available as an aqueous dispersion, and has been widely used in ECDs in conjunction with metal oxides or viologens. Aqueous processability has also been achieved in other undoped ECPs in the form of polyelectrolytes, *i.e.* containing ionic groups such as sulfonate and carboxylates on the side chains.^{233–235} However, aqueous solution-based fabrication has problems with drying time, morphology control, and interfacing with aqueous electrolytes due to their enhanced solubility. A recent report on a ProDOT-based system consisting of carboxylate side chains has shown to be processable from water, and subsequently made aqueous electrolyte compatible with a mild acid wash.²³⁶ An alternate compromised strategy is to use polar functional groups such as ethers, esters and amides on the side chains of conjugated polymers that render processability in benign polar organic solvents, such alcohols and acetates, but afford electroactivity when interfaced with aqueous electrolytes.^{237–239}

4.4 Emerging electrochromic materials

Several classes of strongly correlated transition metal oxides exhibiting metal-insulator transition (MIT) properties have been reported for inducing electrochemically triggered colour changes. For example, the prototypical vanadium dioxide exhibits a near room-temperature metal-insulator transition, between a high temperature stable, metallic VO₂ that adopts tetragonal rutile structure (R-VO₂), and a room temperature stable, insulating phase of VO₂ that adopts monoclinic structure (M1-VO₂).^{240–243} The transition in electrical conductivity between the rutile and monoclinic phases of VO₂ is accompanied by a change in optical reflectance in the near infrared region.²⁴⁴ Electrochemically driven optical transition of the metal-insulator transition materials has been demonstrated using mesoporous VO₂ particle films,¹⁶¹ and another strongly correlated transition metal oxide, samarium nickelate (SmNiO₃), exhibiting metal-insulator transition at 403 K,²⁴⁵ has been demonstrated to undergo transition under external bias mediated by salt water.²⁴⁶ Although the switching kinetics of the metal-insulator transition materials are correlated to the oxygen vacancy formation and structural change,^{244,246} such findings have significantly expanded the library of materials that can be utilised

as electrochromic materials for optical changes in the infrared region.

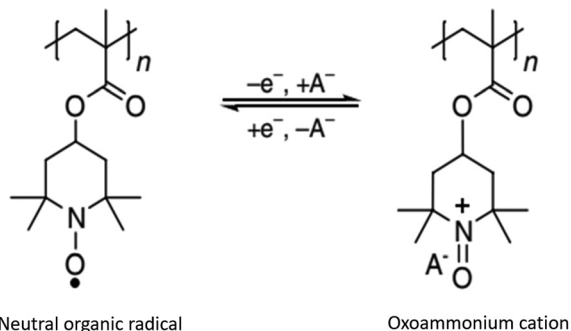
Several other kinds of functional materials with emerging electrochromic properties are also reported, including microporous metal-organic frameworks,^{247,248} organic-halide hybrid perovskites,²⁴⁹ and two dimensional MXenes.²⁵⁰ Composite materials blending two or more electrochromic materials also serve as common strategies for designing electrochromic layers with enhanced properties.^{251–256} While the specific electrochromic mechanisms, especially for emerging electrochromic materials, may require further studies, the synergy arising from their energy storage functions and electrochromic properties offer opportunities for multifunctional devices including electrochromic batteries,^{257,258} supercapacitors,^{259,260} and self-powered electrochromic windows.^{261,262}

5. Counter electrode materials

The counter electrode (ion storage layer) balances the charges consumed at the electrochromic working electrode, through a redox event opposing that occurring at the working electrode. The use of a counter electrode enables the ECD to operate in a smaller voltage range to achieve faster switching with high contrast and long-term stability.²⁶³ The choice of an appropriate counter electrode material mainly depends on its electrochromic properties, which can be categorised as complementary, non-colour changing, and minimally colour changing (MCC) counter electrode materials.

Complementary counter electrode materials have colouration efficiencies comparable to that of the working electrode, and exhibit a noticeable electrochromic performance in the device.^{264,265} In this configuration, the counter electrode material is required to change the colour from a coloured state to a bleached state (or from bleached to coloured) simultaneously as the working electrode material changes from a coloured to a bleached (or bleached to coloured) state. For example, nickel oxide (NiO) a commonly reported anodically colouring electrochromic oxide,²⁶⁶ which can be used as the complementary counter electrode for cathodically colouring WO₃ based ECDs. During the application of cathodic potential to the WO₃ electrode, the WO₃ layer changes from transparent to deep blue, while the NiO counter electrode changes from transparent to brown/black. Both WO₃ and NiO electrodes switch back to the colourless state upon reversal of the applied potential. Similarly, anodically colouring polymers have also been integrated as counter electrode materials in dual electrochromic systems.²⁶⁷ In both cases, the ECD presents colour residue (bleached state) and additive colour (coloured state) of both the working electrode and counter electrode, resulting in a lower device optical contrast when compared to the optical contrasts of each individual electrode.³⁹

Non-colour changing counter electrode materials are electrochromically inactive in the visible wavelength region; *e.g.* the nitroxyl based radical polymer, poly(2,2,6,6-tetramethylpiperidinyloxy-4-yl) (PTMA) (Scheme 1).²⁶⁸ The redox active



Scheme 1 Chemical structures of PTMA in its neutral radical and cationic states. Reprinted with permission from ref. 268. Copyright 2018 Springer Nature.

nitroxyl radical groups are attached to the nonconjugated poly(methyl methacrylate) (PMMA) backbone, which makes this material highly transparent in both redox states (radical and oxoammonium cation). However, high optical contrast and stable redox cyclability of PTMA materials is hindered by the dissolution of the polymer during the redox reactions, which is observed as de-lamination of the device occurring simultaneously with decreased optical contrast upon cycling.²⁶⁹ To stabilise the PTMA based radical polymers during the redox reactions, synthetic strategies including the use of polymer blends (PTMA/PMMA) and crosslinkable block copolymer PTMA-co-(4-benzoyl-phenyl methacrylate) (PTMA-co-BP) have been proposed to address the dissolution problem and to achieve a high optical contrast.^{80,270} However, while polymer blends composed of electrochemically inactive components increases the stability of the active PTMA, it decreases the redox activity of the counter electrode, which in turn necessitates a high voltage range for colour switching of the device. The crosslinkable radical polymer PTMA-co-BP allows colour switching in a smaller voltage window with high optical contrast. Further, both the polymer blend PTMA/PMMA and the crosslinkable PTMA-co-BP require a pre-oxidation step prior to device assembly, when paired with cathodically colouring electrochromic polymers, hindering application of these polymers as counter electrode materials for p-type electrochromic materials.

The third class of counter electrode materials is the minimally colour changing materials that present a low colouration efficiency in the visible wavelength region. Owing to their low colouration efficiency, only minor changes in visible colour are obtained by consuming/generating a large amount of charge during the redox reactions, making these materials useful for compensating the charges of the high colouration efficiency electrochromic materials. As discussed in Section 3.2, the neutral and fully oxidised states of *N*-alkyl-substituted PProDOP absorbs at UV and NIR regions, respectively, leading to a low colouration efficiency ($\sim 35 \text{ cm}^2 \text{ C}^{-1}$) in the visible wavelength region. Thus, it has been widely used as the minimally colour changing counter electrode material for a variety of ECPs that have colouration efficiencies of $\sim 600 \text{ cm}^2 \text{ C}^{-1}$,⁴⁹ and demonstrated excellent stability with optical contrast of $\sim 40\%$.²⁷¹ A potential hurdle towards the large scale application of the MCCP materials is associated with the additional step of pre-oxidation before the

device assembly, as MCCP films in their as-cast state do not exhibit the best performance.²⁶³

In addition to the polymer based counter electrode materials, a large body of cathodically colouring transition metal oxides have relatively low colouration efficiencies on the order of $10 \text{ cm}^2 \text{ C}^{-1}$, and undergo stable ion intercalation/de-intercalation processes that provide significant ion storage capacities. As an alternative to the aforementioned anodic electrochromic transition metal oxide NiO, minimally colour changing transition metal oxides that transform from a transparent state to coloured state under reducing potentials (cathodic colouration) have also been used as counter electrode materials for polymeric ECDs.^{272–274} Because of the minimised colouration efficiencies of the MCC transition metal oxide materials, the colour change in counter electrode component is minimal and does not interfere significantly with the device optical contrast. For example, niobium oxide nanostructures that exhibit high structural stability during Li intercalation and de-intercalation process and low colouration efficiency²⁷⁵ have been demonstrated as minimally colour changing transition metal oxides on counter electrodes, to balance the charge flow during the electrochromic processes without inducing much colour change at the counter electrode.²⁷⁴ The optical purity of the ECDs can be further improved if working electrode and counter electrode are paired in an unbalanced configuration (Fig. 14).²⁷² For example, amorphous WO_3 counter electrode, which has a charge density of $\sim 20 \text{ mC cm}^{-2}$, was used to the balance the charge of the ECP with charge density 2 mC cm^{-2} . In the operation of an ECD, only a small fraction of the charge for achieving full colouration is needed from the counter electrode, which causes it to have a minimal colour change, so the colour purity of the working electrode can be maintained in the ECDs.

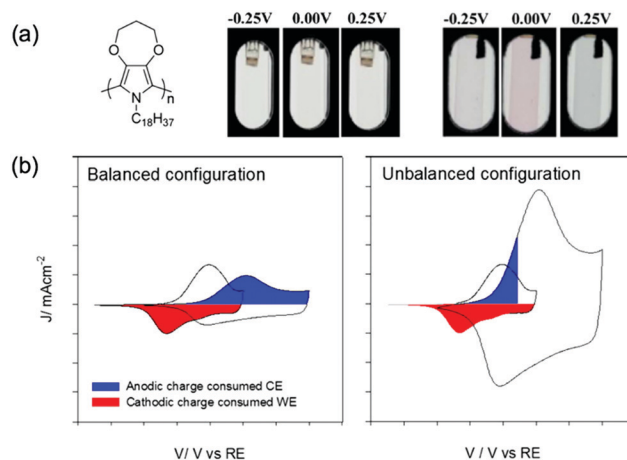


Fig. 14 Use of polymers and metal oxides as counter electrode materials. (a) Films of a minimally colour changing polymer (MCCP) with two different thicknesses (70 nm and 343 nm) at different redox states. Reprinted with permission from ref. 49. Copyright 2012 Royal Society of Chemistry. (b) Cyclic voltammograms of the balanced and unbalanced configurations of ECDs made of PProdot-Me₂/WO₃. Reprinted with permission from ref. 272. Copyright 2016 Elsevier.

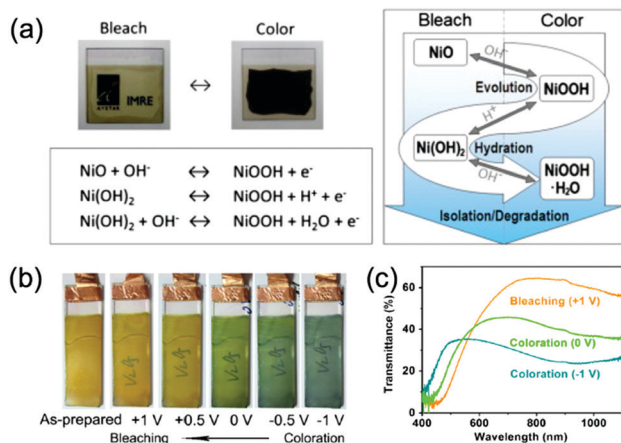


Fig. 15 (a) Anodically colouring NiO, reprinted with permission from ref. 266. Copyright 2013 Elsevier. (b and c) Intermediate (cathodic and anodic) colouring electrochromic V₂O₅, reprinted with permission from ref. 276. Copyright 2015 Elsevier.

Future materials optimisation and exploration for the MCC transition metal oxides require understanding of the structure–property relationship to optimise the charge capacity, electrochromic properties, as well as chemical and electrochemical stability of the counter electrode materials. Because the requirements of MCC counter electrode material share many parallels with that of the Li ion battery cathode materials, understanding of the structure–property relationship of prototypical Li ion battery materials helps rationalizing the design rules for MCC transition metal oxides. For instance, intermediate-type vanadium pentoxide (V₂O₅) materials are both cathodically and anodically colouring (Fig. 15),^{111,276} and are widely used as a cathode material in Li ion battery for their high charge capacitance stemming from reversible and fast transformations between several structurally related, compositionally different Li_xV₂O₅ phases, as the layer-based structure of V₂O₅ allows for feasible intercalation of proton or alkali metal ions concomitant with electron injection,^{277,278} although irreversible phase transformations occur at more reducing potentials. Both crystallographic^{279,280} and morphological engineering^{259,281,282} strategies have been demonstrated to address the irreversible deformation of the materials by facilitating the ion intercalation and de-intercalation processes, leading to higher charge densities, faster switching time and prevent the fracturing and delamination of the oxide structures.

Solution-based processing methods for polymeric counter electrode materials highly depend on the specific properties of the polymer. While radical polymers can be processed using solution based methods, the additional pre-oxidation step limits the scalability of the fabrication, as electrochemical pre-oxidations are typically performed in liquid based electrolytes.^{80,268–270} Moreover, strategies for addressing the dissolution problems observed in the radical polymers require additional steps of optical crosslinking or blending of composite materials, that increases fabrication time and/or cost.²⁷⁰ For MCCP based polymers, electrochemical pre-oxidation

processing is also required, and oxidation of the as-cast polymers in ambient conditions induces difficulties in the control of their electrochemical performances.²⁶³ For inorganic transition metal oxide based nanomaterials and thin films, the solution processability has been demonstrated, often combined with ligand stripping,¹³³ optical processing²⁷⁴ and thermal annealing,¹⁶¹ which also increase fabrication cost. Solution processable synthesis and processing are necessitated for both polymeric and inorganic counter electrode materials to achieve commercial-grade solid-state electrochromic devices.

6. Electrolyte materials

In the multi-layer structured solid-state electrochromic device shown in Fig. 1, the solid (gel) electrolyte layer functions as the separator and adhesive layer while providing the ionic conduction. Different categories of electrolytes, including organic, inorganic, and organic–inorganic hybrid have been reviewed by many groups in energy storage devices, and their applications in the ECDs have also been discussed by Lu *et al.*^{105,283,284} Herein, we mainly focus on the polymer-based electrolytes, and the evaluation of their physical and chemical properties from the perspective of assembly and performance of the multi-layered ECDs.

In typical device assembling procedures as illustrated in Fig. 16, electrochromic thin films and ion storage layers are coated on transparent conducting electrodes to fabricate working electrode and counter electrode, respectively. The electrolyte is selectively drop-casted on either electrode based on its wettability. Several protocols have been established for this process, and they can be classified based on how the electrolyte forms a thin film and establishes the electrode/electrolyte interfaces.

Polymer based electrolyte layers processed *via* solvent casting are typically employed in literature, including polyvinyl alcohol (PVA), poly(vinylidene fluoride-*co*-hexafluoropropylene) (PVDF-HFP), poly(methyl methacrylate) (PMMA), and polyethylene oxide (PEO).^{285–288} In the solvent casting process, the polymers, solvent plasticisers (*e.g.* propylene carbonate, acetonitrile) and salts (*e.g.* LiTFSI, LiClO₄) are dissolved in a low-boiling point solvent, and the mixture is heated up for partial removal of the solvent to form a gel (Fig. 16b). The gel is then directly deposited to either the working or counter electrode to construct ECDs (Fig. 16c and f). A few challenges arise during the electrolyte layer fabrication process. For example, the low boiling point solvents need to be chemically compatible with both the working and counter electrode to ensure functionality of both components in assembled devices. The residue solvent needs to be stringently controlled to avoid the batch-to-batch variation of device performance. Most importantly, the highly viscous polymer gels are non-Newtonian fluids which show complex correlations with the shear force. Finding the suitable large-scale, cost effective and highly efficient printing techniques remains to be a challenge.²⁸⁹

To avoid the above-mentioned issue, an alternative, solvent-free method for fabricating uniform cross-linkable electrolytes

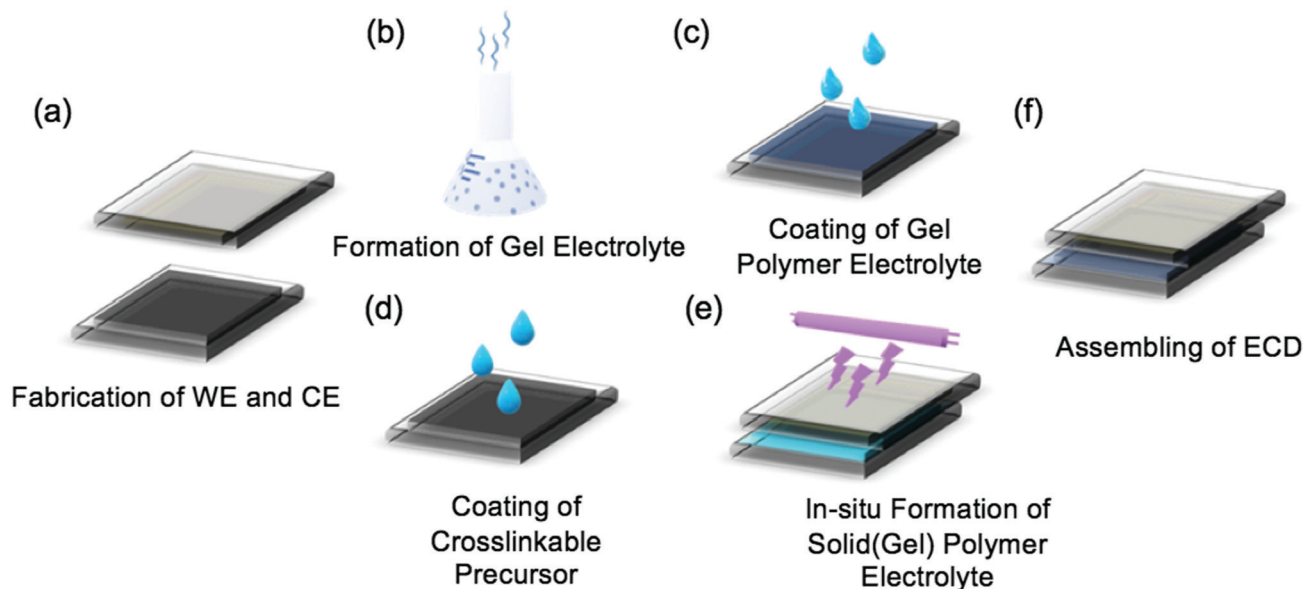


Fig. 16 Schematic representation of steps followed when fabricating the electrolyte layer of an ECD. (a) As-fabricated WE and CE. (b) Evaporation of solvent to form gel electrolyte. (c) Gel polymer electrolyte applied on either WE or CE. (d) Coating of the cross-linkable electrolyte precursor. (e) Photo-/thermal crosslinking of cross-linkable precursor to form solid(gel) polymer electrolyte. (f) Assembling the working and counter electrodes on either side of the electrolyte to fabricate the ECD.

consisting of organic monomers (*e.g.* MMA, PEGDA, and derivatives) and dissolved salts are considered (Fig. 16d). Plasticisers like propylene carbonate can also be blended with the monomer/salt solution, and the *in situ* formation of polymer gel electrolyte can be triggered by heat or UV light (Fig. 16e and f).²⁹⁰ One major issue of the electrolyte layer formed *via in situ* cross-linkable method is the volume contraction, which causes the instability of the electrode/electrolyte interfaces and leads to the decreased stability of ECDs. The volume contraction originates from (1) chemical contraction, where the change of shorter double bonds to longer single bonds during crosslinking process leads to volume shrinkage of the electrolyte, (2) thermal contraction, as the interfaces between the electrolyte and the working/counter electrode are stabilised during the thermal crosslinking process, where thermal expansion takes place, a subsequent decrease in volume occurs after being cooled down to the room temperature, and (3) post-contraction, where residue active sites that remain unreacted during the crosslinking process become further crosslinked over time.²⁹¹ Therefore, to achieve reproducible and stable performance of the electrochromic materials, efforts in both molecular and electrolyte interface design are needed to solve the volume contraction problems in electrolyte layers fabricated by *in situ* crosslinking. An example for another type of monomer-based electrolyte is the organic-inorganic composite ormolyte synthesised *via in situ* sol-gel reactions. Dahmouche *et al.* mixed monomer 3-isocyanatopropyltriethoxysilane, *O,O'*-bis(2-aminopropyl)polypropyleneglycol with lithium salts to prepare the sol-gel precursor, where PEG ionic conductive spacers are inter-connected by -Si-O-Si- bonds. The as-deposited solid-state electrolyte exhibits an ionic conductivity of $10^{-6} \Omega^{-1} \text{cm}^{-1}$ at room temperature.²⁹² A drawback of the ormolyte based electrolyte, however, is the residual

by-product (*e.g.* methanol, ethanol, HCl) generated during the sol-gel reactions, which could be detrimental to the electrochemical stability of the electrochromic materials.

Additionally, inorganic electrolytes like transparent lithium phosphorus oxynitride (LiPON) are often used for all-inorganic electrochromic devices. LiPON presents high electrochemical and physical stability. Moreover, it is highly transmissive and has an ionic conductivity in the order of $\sim 10^{-6} \text{S cm}^{-1}$. However, they are not compatible with low-temperature, solution-processing fabrication methods. Magnetic sputtering has been widely used for the LiPON processing, and has been integrated into the in-line roll-to-roll fabrication methods, although the high-cost of the set-up and the low-processing capacity need to be considered for the commercialisation of the ECDs.²⁹³

7. Aspects of roll-to-roll processing

As previously hinted, ECDs have demonstrated potential to be turned into low-cost printable assemblies as roll-to-roll (R2R) manufactured electronics. Given their stacked nature, however, the all-printed devices remain a challenge to be materialised. The performance metrics discussed above have achieved milestones on wafer-size devices, mainly processed using spin-coating or spray-coating techniques in laboratories, but these performances are yet to transition into meters-long devices. This leap, if made a reality, will enable ECDs to realise their full potential as low-cost flexible electronics. The holdup has mainly been due the fact that ECDs are composed of multiple layers in a stacked configuration, within which each interface can be crucial to the overall device performance. Besides, the ink properties between the stacked layers tend to vary

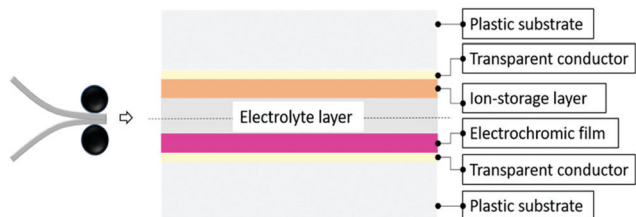


Fig. 17 Lamination approach enabling the roll-to-roll (R2R) manufacturing of ECDs.

immensely, and the integration into a single web-line process becomes difficult. To circumvent this roadblock, a lamination approach as shown in Fig. 17 has been proposed. Principally, the ECD is considered as a two-sided sandwich assembly *i.e.* the colour-changing side and the ion-storage side, separated by the electrolyte layer. This approach thus allows the coating of individual layers, and through a post processing step, the two sided can be brought together as a laminate. This approach enables the investigation of engineering and chemistry know-how that are needed for each layer and interface. In the following section, we first highlight deposition techniques that have shown to be compatible with different layers in ECDs, and then discuss the choice of substrates adaptable to R2R manufacturing.

7.1 Deposition techniques

For laboratory scale studies, spin coating and spray coating are used as quick deposition techniques for small-scale substrates.²⁹⁴ To deposit thin-films onto moving substrates, a continuous supply of the ink is warranted, and is to be matched up with the web speed. Combinatorial studies on ink properties and web rolling to enable the transition from wafer-scale to meters-long rolls have gained a great deal of attention, and still constitute a large aspect of the next step towards the commercialisation of printed devices. For ECDs manufacturing, the deposition technique will vary in accordance to the ink properties *i.e.* viscosity, drying rate, *etc.*, and these properties may vary from layer to layer. Molecular designs enabling solution-processable electrochromic polymers have been extensively studied and discussed above. For inorganic materials, which are typically deposited thermally or by sputtering,^{295,296} our discussion will be applicable to sol-gel processable inks^{297,298} that are readily compatible with plastic substrates used in R2R. We do note, however, that sputtering units can be appended onto the R2R machines given the compatibility with the flexible substrates. But such features usually require either high vacuum (closed chamber setup) or high purity gas flow (open chamber), which can significantly increase the cost.

In this review, we only highlight works that utilised slot-die coating, inkjet printing, and gravure printing as representative techniques that have shown promising outcomes approaching commercialisation quality film deposition (Fig. 18).²⁹⁹ In all these deposition methods, the goal is to uniformly deposit a thin film as the web line moves, allow for any necessary molecular packing or self-assembly, then dry before collecting

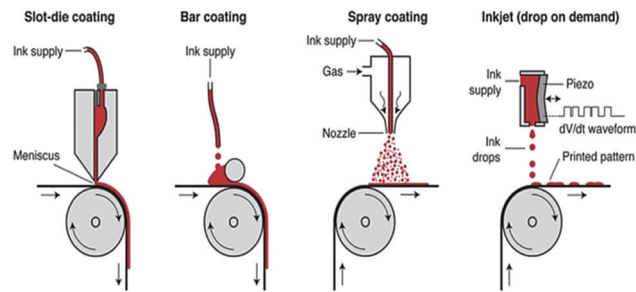


Fig. 18 Several ink deposition techniques used for R2R processing of ECDs. Reprinted with permission from ref. 299. Copyright 2015 John Wiley and Sons.

the coated web. In slot-die coating, the ink is supplied through a miniscule opening orthogonal to the moving substrates forming a meniscus, and the extra ink is wiped away by the back lip. The ink supply is typically controlled by an external pump to continuously fill the die-head. The coating gap between the die-head and the substrates is typically small, as the resulting thickness is estimably half of the coating gap. Slot-die is commonly suitable for low viscosity inks, which can be continuously dispensed through the die-head. For these reasons, slot-die has shown to be an excellent technique to deposit electrochromic polymers, whose layers are typically a few hundreds of nanometres thick. For extremely low viscosity inks, difficulties tend to rise as the die-head is no longer able to contain the solution. In such cases, other techniques or the use of additives to increase the viscosity would be needed. A common remedy for low viscosity scenarios is using gravure printing. In gravure coating, commonly, the ink solution is contained in a well and is picked up by a rotating roller to bring it in contact with a gently touching web. The thickness is now controlled by the roller pick-up speed, the web speed, and the ink viscosity. Gravure printing thus enables coating a wider range of inks as well as a wide range of thickness. Fig. 19 shows high quality films of ECP-magenta coated using both slot-die

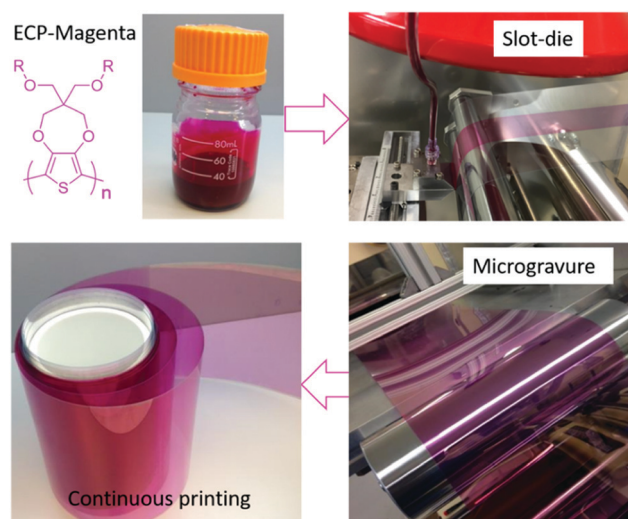


Fig. 19 Printing of ECP-magenta with slot-die and microgravure coating.

coating and microgravure using R2R. The wet films could be passed through a drying chamber and meters long rolls could be collected.

7.2 Substrates

Polyethylene terephthalate or naphthalate (PET or PEN) and polyimide-based substrates are commercially available in the forms of meters-long webs for R2R setups. Owing to their mechanical durability and optical transparency, PET and PEN serve as great candidates for the winding and unwinding during the printing. Machine precision has also been developed to reduce any vibrations along the web line. Frictional force along the press-on rolls is also to be considered as the substrate moves along the commonly-used stainless rolls. Friction is commonly minimised by precisely adjusting the web tension, as well as controlling the web speed. Since the development of plastic substrates is much more matured, the challenging part in this regard is to coat the roll with highly conductive inks.

ITO, as it is the case for glass substrates, is the most commonly used conductor on flexible substrates. But these substrates are costly and exhibit relatively high sheet resistance (35 Ohm sq^{-1} for PET/ITO), which has incited the search for cost-effective and more flexible alternatives. Metal (*i.e.* silver) wire grids have been studied as alternative transparent conductors.^{300,301} These metal grids could further be embedded into semiconducting polymer films (*e.g.* PEDOT:PSS), enabling the printing of cost-effective conducting films for all-polymer ECDs. Other alternatives include graphene, but it imposes a larger sheet resistance ($>1 \text{ k}\Omega \text{ sq}^{-1}$) for practical applications.³⁰²

8. Current status, challenges, and proposed solutions

While the field of electrochromic materials continues to progress, there remains a few scientific and technological challenges that need to be addressed by both materials optimisation/exploration and device engineering methods, to further improve the optical performance and stability of the ECDs in order to meet the demands of large-scale, cost-effective and commercialised applications.

8.1 Ion-trapping

As mentioned in the introductory section, the electron oxidation/reduction processes of both the polymer and the transition metal oxide based electrochromic films are accompanied by counter-ion de-/intercalations to maintain charge-neutrality. Literature reports of both transition metal oxides^{303–306} and polymer based electrochromic layers^{307,308} indicate a decrease of the optical contrast upon repeated cycling, along with a decrease in charge density. In metal-oxide based electrochromic materials, this phenomenon has been attributed to counter-ions being bound to trap-sites, and the concentration, site, and depth-dependent distribution are affected by both the intrinsic properties of the materials and the protocols of voltammetric cycling.³⁰⁶ Application of sufficient overpotentials for long

periods have been able to drive out ions in “shallow” traps, reviving the performance to a certain extent.³⁰³ In electrochromic conjugated polymers, both cations and anions are trapped and absorbed on polymers to form compact and dense microstructures, which prevents further intercalation of counterions, resulting in less electroactive sites. Cycling performance can be improved by forming a more porous morphology,³⁰⁷ reducing the interaction time between polymers and counterions by using a lower concentration of electrolyte, applying a smaller voltage, or reducing the anodic or cathodic polarisation time. However, decreasing the interaction between polymers and counterions also leads to the decrease of the optical contrast. Up to now, the strategies investigated for both inorganic and organic materials do not provide a permanent solution. Further investigations are warranted for the study of the ion-trapping phenomena and the design of EC materials with minimum trap sites.

8.2 Optical memory

The optical memory describes the tendency of the electrochromic materials to maintain its coloured or bleached states after removing the external bias.¹¹ Self-bleaching properties are commonly observed in small molecule based ECDs, in which the small molecules can easily diffuse into electrolyte and undergo electron transfer.³⁰⁹ For conjugated polymer electrochromic materials, self-bleaching and self-colouring^{310,311} phenomena have also been observed due to the spontaneous electron transfer from the ECPs to the transparent conductive substrates. In order to maintain the optical state of the ECDs, refreshing potential pulses can be applied, which increases the power consumption of the devices.

While side-chain modifications of the electrochromic polymers could effectively tune the HOMO levels of the electrochromic materials to address the self-bleaching issue, chemical modifications inevitably change their colour and electrochemical properties.³¹² Alternatively, a general protocol with the combination of cathodic polarisation and surface modification of the ITO electrodes has been proposed to minimise the self-bleaching of ECPs, as cathodic polarisation closes up the opening conformation of ECPs after electrochemical conditioning, while partial surface modifications impede the spontaneous charge transfer between the ECPs and the ITO substrates.³¹¹

8.3 Electrochemical conditioning

Oftentimes, an electrochromic polymer needs to undergo an initial electrochemical redox cycling process to attain the appropriate morphology that results in the optimum electrochemical performance. As a common observation during laboratory measurements of the electrochemical properties of conjugated electrochromic polymers, the charge density of the electrochromic curve typically increases during the initial tens of cycles before its stabilisation. This initial difference in electrochemical response is typically phrased as the memory, first cycle effect, or the electrochemical conditioning process.^{231,313} Both microscopic and electrochemical studies indicate that the change in electrochromic polymer thin film morphologies leads

to the electrochemical conditioning processes that are observed during the initial electrochemical measurements.^{311,314–316} Heinze *et al.* proposed a different model to describe the memory effect based on a study using a polypyrrole system. In the beginning of the charging process of polypyrrole, the formation of σ -dimers impedes the motion of the anions. As a result, the cations are incorporated into the polymers to maintain the electroneutrality in the following discharging process, which leads to the memory effect.^{317,318}

8.4 Residual colour and black-to-transmissive switching

When designing polymers to switch between coloured and transmissive states, as required for window applications, it is crucial that the absorption of the doped state does not overlap or tail into the visible region, so that a residual colour is not observed in the transmissive state. This is increasingly difficult for high bandgap yellow, orange and red polymers, as high potentials may be required for complete bleaching. The higher potentials may cause devices to show slow and incomplete transitions, as well as decreased lifetime. An alternative strategy is to use anodically colouring materials, which are already transmissive in the neutral state with oxidation leading to colouration. However, the presence of the intermediate colours, as mentioned before, makes it not suitable for most applications, and similar issues related to the cathodically colouring polymers may be encountered.

Although colour tuning for a specifically coloured polymer can be achieved based on the understanding of polymer compositions and structures, obtaining a polymer that can be switched between black and transmissive state can be nontrivial, as it requires high absorption over the visible region in the neutral state, and suppression of the absorbance in the bleached state. The reversible and controlled tuning of such broad absorption has been demonstrated using triarylamine based polymers, donor–acceptor based conjugated polymers,^{21,216} colour mixing blends³¹⁹ or multi-layers of electrochromes that cover the whole visible spectrum.^{319,320} However, challenges in controlling the optical contrast, switching time, and uniformity of colour transition for the black-to-transmissive switching ECPs may arise when using these approaches.

8.5 Environmental stability

The primary application of ECDs are electrochromic windows that can be integrated to buildings for energy saving purposes. However, the high production cost has become one of the biggest barriers to market penetration.³²¹ One way to compensate the high cost is to extend their lifespan and save energy in the long run. In general, lifetimes greater than 20 years are targeted for energy saving applications. To achieve long-term stable performances, the thermal and photo- stabilities of the ECDs need to be considered. Unfortunately, investigations on the thermal stability of the ECDs are scarce and not many conclusions and clues from the instability of materials at high-temperature have been drawn.³²² One factor that plays an important role in multiple layered ECDs is the thermal expansion coefficients. Different components integrated within

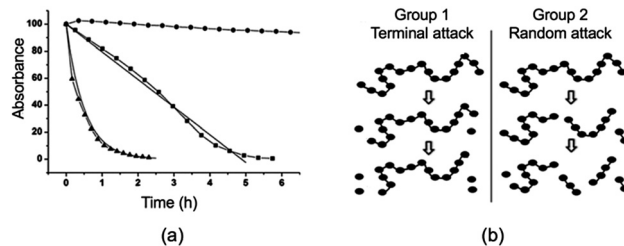


Fig. 20 (a) Variation of the normalised maximum absorbance of three different ECP thin-films (ECP-orange, ECP-magenta and ECP-blue in order of increasing stability) as a function of solar irradiation time, (b) schemes of photoelectrochemical degradation mechanisms of ECPs. Adapted with permission from ref. 324. Copyright 2013 Royal Society of Chemistry.

a single electrochromic device can have very different thermal coefficients, which causes problems in mechanical and physical stabilities upon heating and cooling cycles.

Photostability of the electrochromic materials is another key factor that determines the lifetime of the ECDs used in outdoor conditions. The photochemical breakdown of the conjugation in the polymers is known as a combinatory effect of oxygen, moisture and light, which induces oxidation of the alkyl side chains, leading to chain scission and/or loss of conjugation in the backbone.³²³ A group of ECPs has been investigated to analyse the effect of the chemical constitution on the photochemical stability (Fig. 20).³²⁴ ECPs with relatively lower lying HOMO levels typically have better photochemical stability, although the position of the HOMO level is not necessarily correlated with the photochemical stability. With the addition of methacrylate functionalities on the side chain, ECP-magenta has a five-fold increase in photochemical stability, which could be attributed to the absorption of high-energy photons by the carbonyl groups and further induced crosslinking reactions. Two main degradation mechanisms have been proposed based on the degradation curves of different ECPs.³²⁴ In the group 1, the ECPs only degrade from the terminal positions, which have fixed number of active sites. Therefore, a linear degradation behaviour can be observed. While in the group 2, there are no preferred attacking sites for these ECPs. As a result, the degradation rate decelerated overtime due to the decreased number of active sites. Photostability issues not only exist in ECPs, but also in metal oxide based electrochromic materials due to photocatalytic and photoelectrochemical reactions in the presence of water and oxygen.^{325–328} To address the issues of the photochemical degradation of electrochromic materials, the encapsulation of devices in an inert atmosphere is required for the fabrication and assembly of the ECDs, which further increase the cost of the device.³²⁹

8.6 Haze and transparency

While the optical properties of the electrochromic and ion storage materials have been extensively studied, the overall device refractive index arising from each component, including the transparent conductive substrate and electrolyte, have been overlooked in reported solid-state ECDs. When light transmits

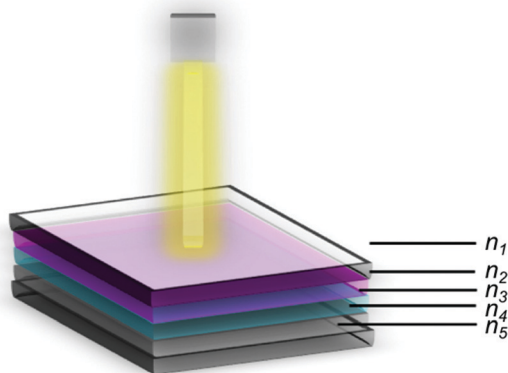


Fig. 21 Schematic representation of a light beam incident normal to a multi-layer ECD surface and the notation of the refractive index of air (n_1) and each layer (n_2 – n_5).

through an interface of two materials with different refractive indexes at normal incidence, the reflected fraction (ρ) is calculated by the following equation:

$$\rho = \left(\frac{n_1 - n_2}{n_1 + n_2} \right)^2 \quad (8)$$

where ρ is the fraction of light that is reflected at the interface, n_1 and n_2 are the refractive indexes of the media before and after the light crosses the interface.

Then, the fraction that is transmitted can be derived as:

$$T = 1 - \rho, \quad (9)$$

where T is the fraction of the light that is transmitted through the interface.

When the device is assembled from m parallel layers, including solution processable materials coated onto substrates, $(m + 1)$ interfaces will be generated. For a typical solid state, five-component ECD, six interfaces will affect the overall optical transmittance of the device. The total transmittance of the electrochromic device can be obtained from the product of the transmittance values at these six interfaces (Fig. 21, eqn (10) and (11)). For certain applications of ECDs, for example, transmittance type electrochromic windows, which require a higher fraction of incoming light to go through the device with higher transmission in the bleached state, the materials for electrolyte should be carefully selected based on their refractive indexes, so that the Δn at each interface can be smaller, which gives a clearer view through the ECD.

$$T_{\text{net}} = T_1 \times T_2 \times T_3 \times T_4 \times T_5 \times T_6 \quad (10)$$

$$T_{\text{net}} = \left[1 - \left(\frac{n_1 - n_2}{n_1 + n_2} \right)^2 \right] \left[1 - \left(\frac{n_2 - n_3}{n_2 + n_3} \right)^2 \right] \left[1 - \left(\frac{n_3 - n_4}{n_3 + n_4} \right)^2 \right] \\ \times \left[1 - \left(\frac{n_4 - n_5}{n_4 + n_5} \right)^2 \right] \left[1 - \left(\frac{n_5 - n_2}{n_5 + n_2} \right)^2 \right] \left[1 - \left(\frac{n_2 - n_1}{n_2 + n_1} \right)^2 \right] \quad (11)$$

Where T_{net} is the net transmittance after passing all layers in ECDs, $T_1, T_2, T_3, T_4, T_5, T_6$ are the fraction of light transmitted at different interfaces in the ECD. n_1, n_2, n_3, n_4, n_5 are the refractive indexes of the media (each layer of materials) in the ECD.

Other than the refractive index mismatch between each layer, the heterogeneity of the refractive indexes for some types of electrolytes, especially semi-crystalline polymers like PVDF, PEO, *etc.*, needs to be noted. For example, PVDF polymers tend to form large crystalline domains during the drying processes, which generate crystalline phases with different crystallographic symmetries and orientations,³³⁰ mixed with amorphous phases. These phases with different crystallinity have different refractive indexes, leading to the formation of a translucent thin film, resulting in a decrease of the optical transparency of the ECDs.

To improve the ionic conductivity of polymer-based electrolytes, inorganic nanoparticles, like SiO_2 , Al_2O_3 , and TiO_2 , are often used as additives to reduce the crystallinity and to increase the motion of the polymer chains. Matching of the refractive indexes between metal oxides and polymer electrolytes is necessary to obtain a transparent electrolyte layer.

9. Closing remarks

We have reviewed and discussed the operating principles, materials design rules and technical roadblocks for the commercialisation of ECDs that are compatible with large-scale processing methods, including the roll-to-roll techniques. Synthesis and processing of materials with excellent electrochromic, charge balancing and transport properties not only requires materials design that consider performance metrics measured by standard laboratory electrochemical and optical methods, but also take into account other parameters including the materials homogeneity, scalability, and stability under device operating conditions, many of which lead to trade-offs between parameters that require in-depth understanding of the device operations.

Several key issues need to be solved when fabricating the next generation of ECDs that are more efficient and stable, based on the understanding of the following questions:

1. How does the electrochromic materials–electrolyte interface vary in physical and chemical aspects as a function of applied potential in real application conditions, for example, at above ambient temperatures in the presence of UV irradiation? Are there experimental or simulation methods that can provide microscopic mechanistic insights into these processes on the molecular or nanoscale?

2. Given the inevitable nature of chemical and electrochemical heterogeneity in the composition, stoichiometry and ordering of the materials especially during large scale synthesis and processes, are there alternative methods to address the inhomogeneity issue? For example, instead of porous thin film electrode materials, can we combine the mechanical robustness of matrix materials and the electrochromic or ion storage properties of the electrochemically active materials, in a highly dispersible

and permeable way that is compatible with current fabrication methods?

3. How could we rationally design and optimally match the chemical, electrochemical, optical and thermal compatibilities between each component of the ECDs, to achieve more stable ECDs with excellent optical performances?

Such questions illustrate the importance of understanding electrochromic materials and device interfaces on the nano-scale, as well as the consideration of synthesis and processing compatibility of each device component in large scale. With the rapid advances in materials science, future progress in the exploration of material properties as a function of synthetic parameters, processing methods, compatibility between components and robustness towards environmental conditions will further inspire the development of ECDs exhibiting outstanding performance.

Conflicts of interest

Dr Jianguo Mei is a co-founder and Scientific Advisor of Ambilight Inc, which is dedicated to roll-to-roll manufacturing of thin film electrochromic products.

Acknowledgements

The authors are grateful for the unrestricted gift from Ambilight Inc.

References

- 1 P. Brühwiler and M. Buyan, *EMPA Act.*, 2005, **5**, 49.
- 2 A. Azens and C. G. Granqvist, *J. Solid State Electrochem.*, 2003, **7**, 64–68.
- 3 F. G. K. Baucke, *Sol. Energy Mater.*, 1987, **16**, 67–77.
- 4 S. K. Deb, *Appl. Opt.*, 2015, **8**, 192.
- 5 S. K. Deb, *Philos. Mag.*, 1973, **27**, 801–822.
- 6 N. A. Chernova, M. Roppolo, A. C. Dillon and M. S. Whittingham, *J. Mater. Chem.*, 2009, **19**, 2526–2552.
- 7 S. K. Deb, *Sol. Energy Mater. Sol. Cells*, 2008, **92**, 245–258.
- 8 R. Li, K. Li, G. Wang, L. Li, Q. Zhang, J. Yan, Y. Chen, Q. Zhang, C. Hou, Y. Li and H. Wang, *ACS Nano*, 2018, **12**, 3759–3768.
- 9 R. J. Mortimer, *Electrochim. Acta*, 1999, **44**, 2971–2981.
- 10 C. M. Amb, A. L. Dyer and J. R. Reynolds, *Chem. Mater.*, 2011, **23**, 397–415.
- 11 P. M. Beaujuge and J. R. Reynolds, *Chem. Rev.*, 2010, **110**, 268–320.
- 12 R. J. Mortimer, *Annu. Rev. Mater. Res.*, 2011, **41**, 241–268.
- 13 R. J. Mortimer, *Chem. Soc. Rev.*, 1997, **26**, 147–156.
- 14 Y. Alesanco, A. Viñuales, J. Rodriguez and R. Tena-Zaera, *Materials*, 2018, **11**, 414.
- 15 C.-G. Granqvist, *Nat. Mater.*, 2006, **5**, 89.
- 16 R. J. Mortimer, *Electrochim. Acta*, 1999, **44**, 2971–2981.
- 17 D. R. Rosseinsky and R. J. Mortimer, *Adv. Mater.*, 2001, **13**, 783–793.
- 18 F. G. K. Baucke, *Mater. Sci. Eng., B*, 1991, **10**, 285–292.
- 19 R. D. Rauh, *Electrochim. Acta*, 1999, **44**, 3165–3176.
- 20 P. Bonhote, E. Gogniat, F. Campus, L. Walder and M. Grätzel, *Displays*, 1999, **20**, 137–144.
- 21 P. M. Beaujuge, S. Ellinger and J. R. Reynolds, *Nat. Mater.*, 2008, **7**, 795.
- 22 A. M. Österholm, D. E. Shen, J. A. Kerszulis, R. H. Bulloch, M. Kuepfert, A. L. Dyer and J. R. Reynolds, *ACS Appl. Mater. Interfaces*, 2015, **7**, 1413–1421.
- 23 T. Deutschmann and E. Oesterschulze, *J. Opt.*, 2014, **16**, 75301.
- 24 H. J. Byker, Gentex Corp, *US Pat.*, 4902108, 1990.
- 25 R. B. Goldner, D. H. Mendelsohn, J. Alexander, W. R. Henderson, D. Fitzpatrick, T. E. Haas, H. H. Sample, R. D. Rauh, M. A. Parker and T. L. Rose, *Appl. Phys. Lett.*, 1983, **43**, 1093–1095.
- 26 H. Demiryont and D. Moorehead, *Sol. Energy Mater. Sol. Cells*, 2009, **93**, 2075–2078.
- 27 U. Bach, D. Corr, D. Lupo, F. Pichot and M. Ryan, *Adv. Mater.*, 2002, **14**, 845–848.
- 28 A. Bessiere, C. Marcel, M. Morcrette, J. M. Tarascon, V. Lucas, B. Viana and N. Baffier, *J. Appl. Phys.*, 2002, **91**, 1589–1594.
- 29 T. Kamimori, J. Nagai and M. Mizuhashi, *Sol. Energy Mater.*, 1987, **16**, 27–38.
- 30 D. A. C. Brownson and C. E. Banks, *The handbook of graphene electrochemistry*, Springer, 2014.
- 31 G. Garcia, R. Buonsanti, E. L. Runnerstrom, R. J. Mendelsberg, A. Llordes, A. Anders, T. J. Richardson and D. J. Milliron, *Nano Lett.*, 2011, **11**, 4415–4420.
- 32 E. L. Runnerstrom, A. Llordés, S. D. Lounis and D. J. Milliron, *Chem. Commun.*, 2014, **50**, 10555–10572.
- 33 N. Elgrishi, K. J. Rountree, B. D. McCarthy, E. S. Rountree, T. T. Eisenhart and J. L. Dempsey, *J. Chem. Educ.*, 2017, **95**, 197–206.
- 34 C. Bechinger, J. N. Bullock, J. Zhang, C. E. Tracy, D. K. Benson, S. K. Deb and H. M. Branz, *J. Appl. Phys.*, 1996, **80**, 1226–1232.
- 35 K. H. Cheng and M. S. Whittingham, *Solid State Ionics*, 1980, **1**, 151–161.
- 36 S. F. Cogan, E. J. Anderson, T. D. Plante and R. D. Rauh, *Appl. Opt.*, 1985, **24**, 2282–2283.
- 37 R. D. Rauh and S. F. Cogan, *J. Electrochem. Soc.*, 1993, **140**, 378–386.
- 38 K. Xu, S. P. Ding and T. R. Jow, *J. Electrochem. Soc.*, 1999, **146**, 4172–4178.
- 39 J. Padilla, V. Seshadri, G. A. Sotzing and T. F. Otero, *Electrochem. Commun.*, 2007, **9**, 1931–1935.
- 40 S. Hassab, D. E. Shen, A. M. Österholm, J. R. Reynolds and J. Padilla, *J. Mater. Chem. C*, 2018, **6**, 393–400.
- 41 J. P. Matthews, J. M. Bell and I. L. Skryabin, *Electrochim. Acta*, 1999, **44**, 3245–3250.
- 42 J. M. Bell, J. P. Matthews and I. L. Skryabin, *Solid State Ionics*, 2002, **152**, 853–860.
- 43 P. K. Shen, K. Y. Chen and A. C. C. Tseung, *J. Electrochem. Soc.*, 1994, **141**, 1758–1762.

- 44 J. B. Craig and J. M. Grant, *J. Mater. Chem.*, 1992, **2**, 521–524.
- 45 W. Kaim and J. Fiedler, *Chem. Soc. Rev.*, 2009, **38**, 3373–3382.
- 46 Y.-M. Zhang, X. Wang, W. Zhang, W. Li, X. Fang, B. Yang, M. Li and S. X.-A. Zhang, *Light: Sci. Appl.*, 2015, **4**, e249.
- 47 A. Watanabe, K. Mori, Y. Iwasaki, Y. Nakamura and S. Niizuma, *Macromolecules*, 1987, **20**, 1793–1796.
- 48 G. A. Sotzing, J. L. Reddinger, A. R. Katritzky, J. Soloducho, R. Musgrave, J. R. Reynolds and P. J. Steel, *Chem. Mater.*, 1997, **9**, 1578–1587.
- 49 E. P. Knott, M. R. Craig, D. Y. Liu, J. E. Babiarz, A. L. Dyer and J. R. Reynolds, *J. Mater. Chem.*, 2012, **22**, 4953–4962.
- 50 B. C. Thompson, P. Schottland, K. Zong and J. R. Reynolds, *Chem. Mater.*, 2000, **12**, 1563–1571.
- 51 K. Nassau, *Color for science, art and technology*, Elsevier, 1997, vol. 1.
- 52 A. L. Dyer, E. J. Thompson and J. R. Reynolds, *ACS Appl. Mater. Interfaces*, 2011, **3**, 1787–1795.
- 53 L. W. Kheng, *Color Res. Appl.*, 2002, **24**, 186–198.
- 54 A. R. Robertson, *Color Res. Appl.*, 1990, **15**, 167–170.
- 55 R. G. McGuire, *HortScience*, 1992, **27**, 1254–1255.
- 56 R. Cortez, D. A. Luna-Vital, D. Margulis and E. Gonzalez de Mejia, *Compr. Rev. Food Sci. Food Saf.*, 2017, **16**, 180–198.
- 57 M. Melgosa, *Color Res. Appl.*, 2000, **25**, 49–55.
- 58 J. Fei, K. G. Lim and G. T. R. Palmore, *Chem. Mater.*, 2008, **20**, 3832–3839.
- 59 R. H. Bulloch, J. A. Kerszulis, A. L. Dyer and J. R. Reynolds, *ACS Appl. Mater. Interfaces*, 2014, **6**, 6623–6630.
- 60 V. Seshadri, J. Padilla, H. Bircan, B. Radmard, R. Draper, M. Wood, T. F. Otero and G. A. Sotzing, *Org. Electron.*, 2007, **8**, 367–381.
- 61 A. Kumar, M. T. Otley, F. A. Alamar, Y. Zhu, B. G. Arden and G. A. Sotzing, *J. Mater. Chem. C*, 2014, **2**, 2510–2516.
- 62 J. Y. Lim, H. C. Ko and H. Lee, *Synth. Met.*, 2005, **155**, 595–598.
- 63 J. Kawahara, P. A. Ersman, I. Engquist and M. Berggren, *Org. Electron.*, 2012, **13**, 469–474.
- 64 G. Cai, M. Cui, V. Kumar, P. Darmawan, J. Wang, X. Wang, A. L.-S. Eh, K. Qian and P. S. Lee, *Chem. Sci.*, 2016, **7**, 1373–1382.
- 65 J. Padilla, A. M. Österholm, A. L. Dyer and J. R. Reynolds, *Sol. Energy Mater. Sol. Cells*, 2015, **140**, 54–60.
- 66 C.-C. Jaing, C.-J. Tang, C.-C. Chan, K.-H. Lee, C.-C. Kuo, H.-C. Chen and C.-C. Lee, *Appl. Opt.*, 2014, **53**, A154–A158.
- 67 C. L. Gaupp, D. M. Welsh, R. D. Rauh and J. R. Reynolds, *Chem. Mater.*, 2002, **14**, 3964–3970.
- 68 E. S. Lee, S. E. Selkowitz, R. D. Clear, D. L. DiBartolomeo, J. H. Klems, L. L. Fernandes, G. Ward, V. Inkarojrit and M. Yazdani, *Advancement of electrochromic windows*, Ernest Orlando Lawrence Berkeley National Laboratory, Berkeley, CA (US), 2006.
- 69 C. G. Granqvist, *Sol. Energy Mater. Sol. Cells*, 2000, **60**, 201–262.
- 70 T. Xu, E. C. Walter, A. Agrawal, C. Bohn, J. Velmurugan, W. Zhu, H. J. Lezec and A. A. Talin, *Nat. Commun.*, 2016, **7**, 10479.
- 71 R. J. Mortimer and J. R. Reynolds, *J. Mater. Chem.*, 2005, **15**, 2226–2233.
- 72 M. Fabretto, T. Vaithianathan, C. Hall, J. Mazurkiewicz, P. C. Innis, G. G. Wallace and P. Murphy, *Electrochim. Acta*, 2008, **53**, 2250–2257.
- 73 R. D. Rauh, F. Wang, J. R. Reynolds and D. L. Meeker, *Electrochim. Acta*, 2001, **46**, 2023–2029.
- 74 M. Fabretto, T. Vaithianathan, C. Hall, P. Murphy, P. C. Innis, J. Mazurkiewicz and G. G. Wallace, *Electrochem. Commun.*, 2007, **9**, 2032–2036.
- 75 D. Vernardou, P. Paterakis, H. Drosos, E. Spanakis, I. M. Povey, M. E. Pemble, E. Koudoumas and N. Katsarakis, *Sol. Energy Mater. Sol. Cells*, 2011, **95**, 2842–2847.
- 76 D. J. Jeong, W.-S. Kim and Y.-E. Sung, *Jpn. J. Appl. Phys.*, 2001, **40**, L708.
- 77 M. Panagopoulou, D. Vernardou, E. Koudoumas, N. Katsarakis, D. Tsoukalas and Y. S. Raptis, *J. Phys. Chem. C*, 2016, **121**, 70–79.
- 78 S. Hassab, D. E. Shen, A. M. Österholm, M. Da Rocha, G. Song, Y. Alesanco, A. Viñuales, A. Rougier, J. R. Reynolds and J. Padilla, *Sol. Energy Mater. Sol. Cells*, 2018, **185**, 54–60.
- 79 A. Kraft, *ChemTexts*, 2019, **5**, 1.
- 80 S. V. Vasilyeva, E. Unur, R. M. Walczak, E. P. Donoghue, A. G. Rinzler and J. R. Reynolds, *ACS Appl. Mater. Interfaces*, 2009, **1**, 2288–2297.
- 81 H. Yu, S. Shao, L. Yan, H. Meng, Y. He, C. Yao, P. Xu, X. Zhang, W. Hu and W. Huang, *J. Mater. Chem. C*, 2016, **4**, 2269–2273.
- 82 M. A. Arvizu, H.-Y. Qu, U. Cindemir, Z. Qiu, E. A. Rojas-González, D. Primetzhofer, C. G. Granqvist, L. Österlund and G. A. Niklasson, *J. Mater. Chem. A*, 2019, **7**, 2908–2918.
- 83 L. Ouyang, B. Wei, C. Kuo, S. Pathak, B. Farrell and D. C. Martin, *Sci. Adv.*, 2017, **3**, e1600448.
- 84 B. Wei, J. Liu, L. Ouyang, C.-C. Kuo and D. C. Martin, *ACS Appl. Mater. Interfaces*, 2015, **7**, 15388–15394.
- 85 Y. Lu, L. Liu, W. Foo, S. Magdassi, D. Mandler and P. S. Lee, *J. Mater. Chem. C*, 2013, **1**, 3651–3654.
- 86 A. Piccolo and F. Simone, *J. Build. Eng.*, 2015, **3**, 94–103.
- 87 T. Chow, C. Li and Z. Lin, *Sol. Energy Mater. Sol. Cells*, 2010, **94**, 212–220.
- 88 M. K. Gunde, U. O. Krašovec and W. J. Platzer, *J. Opt. Soc. Am. A*, 2005, **22**, 416–423.
- 89 C. I. de l'Eclairage, CIE publ.
- 90 N. Aste, F. Leonforte and A. Piccolo, *Sol. Energy*, 2018, **176**, 51–61.
- 91 I. E. S. of N. America, IES TM-30-15.
- 92 N. L. Sbar, L. Podbelski, H. M. Yang and B. Pease, *Int. J. Sustainable Built Environ.*, 2012, **1**, 125–139.
- 93 B. Paule, E. Sok, S. Pantet and J. Boutiller, *Energy Procedia*, 2017, **122**, 199–204.
- 94 A. Piccolo, *Energy Build.*, 2010, **42**, 1409–1417.
- 95 M. Casini, *Renewable Energy*, 2018, **119**, 923–934.
- 96 G. Garcia, R. Buonsanti, A. Llordes, E. L. Runnerstrom, A. Bergerud and D. J. Milliron, *Adv. Opt. Mater.*, 2013, **1**, 215–220.

- 97 H. Gu, C. Guo, S. Zhang, L. Bi, T. Li, T. Sun and S. Liu, *ACS Nano*, 2018, **12**, 559–567.
- 98 D. Arasteh, H. Goudey, J. Huang, C. Kohler and R. Mitchell, *ASHRAE Trans.*, 2007, **113**, 176–186.
- 99 G. B. Smith, C. A. Deller, P. D. Swift, A. Gentle, P. D. Garrett and W. K. Fisher, *J. Nanopart. Res.*, 2002, **4**, 157–165.
- 100 P. M. Beaujuge and J. R. Reynolds, *Chem. Rev.*, 2010, **110**, 268–320.
- 101 W. Wu, M. Wang, J. Ma, Y. Cao and Y. Deng, *Adv. Electron. Mater.*, 2018, **4**, 1800185.
- 102 G. Cai, J. Wang and P. S. Lee, *Acc. Chem. Res.*, 2016, **49**, 1469–1476.
- 103 A. Agrawal, R. W. Johns and D. J. Milliron, *Annu. Rev. Mater. Res.*, 2017, **47**, 1–31.
- 104 C. M. Amb, A. L. Dyer and J. R. Reynolds, *Chem. Mater.*, 2010, **23**, 397–415.
- 105 V. K. Thakur, G. Ding, J. Ma, P. S. Lee and X. Lu, *Adv. Mater.*, 2012, **24**, 4071–4096.
- 106 A. L. Eh, A. W. M. Tan, X. Cheng, S. Magdassi and P. S. Lee, *Energy Technol.*, 2018, **6**, 33–45.
- 107 C. G. Granqvist, M. A. Arvizu, İ. B. Pehlivan, H.-Y. Qu, R.-T. Wen and G. A. Niklasson, *Electrochim. Acta*, 2018, **259**, 1170–1182.
- 108 C. G. Granqvist, *Appl. Phys. A: Mater. Sci. Process.*, 1993, **57**, 3–12.
- 109 B. Gerand, G. Nowogrocki, J. Guenot and M. Figlarz, *J. Solid State Chem.*, 1979, **29**, 429–434.
- 110 R. J. Colton, A. M. Guzman and J. W. Rabalais, *Acc. Chem. Res.*, 1978, **11**, 170–176.
- 111 C. G. Granqvist, *Handbook of inorganic electrochromic materials*, Elsevier, 1995.
- 112 J. M. Berak and M. J. Sienko, *J. Solid State Chem.*, 1970, **2**, 109–133.
- 113 L. Su, L. Zhang, J. Fang, M. Xu and Z. Lu, *Sol. Energy Mater. Sol. Cells*, 1999, **58**, 133–140.
- 114 D. T. Gillaspie, R. C. Tenent and A. C. Dillon, *J. Mater. Chem.*, 2010, **20**, 9585–9592.
- 115 C. G. Granqvist, *Sol. Energy Mater. Sol. Cells*, 2012, **99**, 1–13.
- 116 B. W. Faughnan, *RCA Rev.*, 1975, **36**, 177–197.
- 117 O. F. Schirmer, V. Wittwer, G. Baur and G. Brandt, *J. Electrochem. Soc.*, 1977, **124**, 749–753.
- 118 G. A. Niklasson and C. G. Granqvist, *J. Mater. Chem.*, 2007, **17**, 127–156.
- 119 R. Chatten, A. V. Chadwick, A. Rougier and P. J. D. Lindan, *J. Phys. Chem. B*, 2005, **109**, 3146–3156.
- 120 S. J. Yoo, J. W. Lim, Y.-E. Sung, Y. H. Jung, H. G. Choi and D. K. Kim, *Appl. Phys. Lett.*, 2007, **90**, 173126.
- 121 S. H. Lee, H. M. Cheong, C. E. Tracy, A. Mascarenhas, A. W. Czanderna and S. K. Deb, *Appl. Phys. Lett.*, 1999, **75**, 1541–1543.
- 122 H.-S. Shim, J. W. Kim, Y.-E. Sung and W. B. Kim, *Sol. Energy Mater. Sol. Cells*, 2009, **93**, 2062–2068.
- 123 K. Miyake, H. Kaneko, M. Sano and N. Suedomi, *J. Appl. Phys.*, 1984, **55**, 2747–2753.
- 124 S. H. Lee, R. Deshpande, P. A. Parilla, K. M. Jones, B. To, A. H. Mahan and A. C. Dillon, *Adv. Mater.*, 2006, **18**, 763–766.
- 125 J. Wang, E. Khoo, P. S. Lee and J. Ma, *J. Phys. Chem. C*, 2008, **112**, 14306–14312.
- 126 A. Azam, J. Kim, J. Park, T. G. Novak, A. P. Tiwari, S. H. Song, B. Kim and S. Jeon, *Nano Lett.*, 2018, **18**, 5646–5651.
- 127 Y. Li, W. A. McMaster, H. Wei, D. Chen and R. A. Caruso, *ACS Appl. Nano Mater.*, 2018, **1**, 2552–2558.
- 128 G. D. Stucky, E. W. McFarland, T. Jaramillo and S. H. Baeck, *Nano Lett.*, 2002, **2**, 831–834.
- 129 T. Maruyama and S. Arai, *J. Electrochem. Soc.*, 1994, **141**, 1021–1024.
- 130 H. M. A. Soliman, A. B. Kashyout, M. S. El Nouby and A. M. Abosehly, *J. Mater. Sci. Mater. Electron.*, 2010, **21**, 1313–1321.
- 131 M. Deepa, A. G. Joshi, A. K. Srivastava, S. M. Shivaprasad and S. A. Agnihotry, *J. Electrochem. Soc.*, 2006, **153**, C365–C376.
- 132 D. Qiu, H. Ji, X. Zhang, H. Zhang, H. Cao, G. Chen, T. Tian, Z. Chen, X. Guo, L. Liang, J. Gao and F. Zhuge, *Inorg. Chem.*, 2019, **58**, 2089–2098.
- 133 S. Cong, Y. Tian, Q. Li, Z. Zhao and F. Geng, *Adv. Mater.*, 2014, **26**, 4260–4267.
- 134 W. J. Lee, Y.-K. Fang, J.-J. Ho, W.-T. Hsieh, S.-F. Ting, D. Huang and F. C. Ho, *J. Electron. Mater.*, 2000, **29**, 183–187.
- 135 J. Svensson and C. G. Granqvist, *Sol. Energy Mater.*, 1984, **11**, 29–34.
- 136 A. Subrahmanyam and A. Karuppasamy, *Sol. Energy Mater. Sol. Cells*, 2007, **91**, 266–274.
- 137 C. G. Granqvist, İ. B. Pehlivan and G. A. Niklasson, *Surf. Coat. Technol.*, 2018, **336**, 133–138.
- 138 A. Agrawal, S. H. Cho, O. Zandi, S. Ghosh, R. W. Johns and D. J. Milliron, *Chem. Rev.*, 2018, **118**, 3121–3207.
- 139 M. Hu, J. Chen, Z.-Y. Li, L. Au, G. V. Hartland, X. Li, M. Marquez and Y. Xia, *Chem. Soc. Rev.*, 2006, **35**, 1084–1094.
- 140 S. Araki, K. Nakamura, K. Kobayashi, A. Tsuboi and N. Kobayashi, *Adv. Mater.*, 2012, **24**, OP122–OP126.
- 141 A. Tsuboi, K. Nakamura and N. Kobayashi, *Chem. Mater.*, 2014, **26**, 6477–6485.
- 142 N. Li, P. Wei, L. Yu, J. Ji, J. Zhao, C. Gao, Y. Li and Y. Yin, *Small*, 2019, **15**, 1–7.
- 143 C. J. Barile, D. J. Slotcavage, J. Hou, M. T. Strand, T. S. Hernandez and M. D. McGehee, *Joule*, 2017, **1**, 133–145.
- 144 T. S. Hernandez, C. J. Barile, M. T. Strand, T. E. Dayrit, D. J. Slotcavage and M. D. McGehee, *ACS Energy Lett.*, 2018, **3**, 104–111.
- 145 G. Boschloo and D. Fitzmaurice, *J. Phys. Chem. B*, 1999, **103**, 3093–3098.
- 146 R. Buonsanti, A. Llordes, S. Aloni, B. A. Helms and D. J. Milliron, *Nano Lett.*, 2011, **11**, 4706–4710.
- 147 S. C. Erwin, L. Zu, M. I. Haftel, A. L. Efros, T. A. Kennedy and D. J. Norris, *Nature*, 2005, **436**, 91–94.
- 148 E. L. Runnerstrom, A. Bergerud, A. Agrawal, R. W. Johns, C. J. Dahlgren, A. Singh, S. M. Selbach and D. J. Milliron, *Nano Lett.*, 2016, **16**, 3390–3398.
- 149 W. Hu, S. Guo, J. P. Gaul, M. G. Boebinger, M. T. McDowell and M. A. Filler, *J. Phys. Chem. C*, 2017, **121**, 15970–15976.
- 150 O. Zandi, A. Agrawal, A. B. Shearer, L. C. Reimnitz, C. J. Dahlgren, C. M. Staller and D. J. Milliron, *Nat. Mater.*, 2018, **17**, 710–717.

- 151 A. Agrawal, I. Kriegel, E. L. Runnerstrom, F. Scotognella, A. Lordes and D. J. Milliron, *ACS Photonics*, 2018, **5**, 2044–2050.
- 152 C. M. Staller, Z. L. Robinson, A. Agrawal, S. L. Gibbs, B. L. Greenberg, S. D. Lounis, U. R. Kortshagen and D. J. Milliron, *Nano Lett.*, 2018, **18**, 2870–2878.
- 153 T. E. Williams, C. M. Chang, E. L. Rosen, G. Garcia, E. L. Runnerstrom, B. L. Williams, B. Koo, R. Buonsanti, D. J. Milliron and B. A. Helms, *J. Mater. Chem. C*, 2014, **2**, 3328–3335.
- 154 A. Dong, X. Ye, J. Chen, Y. Kang, T. Gordon, J. M. Kikkawa and C. B. Murray, *J. Am. Chem. Soc.*, 2011, **133**, 998–1006.
- 155 E. L. Rosen, R. Buonsanti, A. Lordes, A. M. Sawvel, D. J. Milliron and B. A. Helms, *Angew. Chem., Int. Ed.*, 2012, **51**, 684–689.
- 156 B. Tandon, A. Agrawal, S. Heo and D. J. Milliron, *Nano Lett.*, 2019, **19**, 2012–2019.
- 157 C. A. Saez Cabezas, G. K. Ong, R. B. Jadrich, B. A. Lindquist, A. Agrawal, T. M. Truskett and D. J. Milliron, *Proc. Natl. Acad. Sci. U. S. A.*, 2018, **115**, 8925–8930.
- 158 A. Lordés, G. Garcia, J. Gazquez and D. J. Milliron, *Nature*, 2013, **500**, 323.
- 159 A. Sakamoto and S. Yamamoto, *Int. J. Appl. Glass Sci.*, 2010, **1**, 237–247.
- 160 G. Garcia, R. Buonsanti, E. L. Runnerstrom, R. J. Mendelsberg, A. Lordes, A. Anders, T. J. Richardson and D. J. Milliron, *Nano Lett.*, 2011, **11**, 4415–4420.
- 161 C. J. Dahlman, G. Leblanc, A. Bergerud, C. Staller, J. Adair and D. J. Milliron, *Nano Lett.*, 2016, **16**, 6021–6027.
- 162 S. Heo, J. Kim, G. K. Ong and D. J. Milliron, *Nano Lett.*, 2017, **17**, 5756–5761.
- 163 X. Guo, M. Baumgarten and K. Müllen, *Prog. Polym. Sci.*, 2013, **38**, 1832–1908.
- 164 A. Facchetti, *Chem. Mater.*, 2010, **23**, 733–758.
- 165 S. Günes, H. Neugebauer and N. S. Sariciftci, *Chem. Rev.*, 2007, **107**, 1324–1338.
- 166 C. Wang, H. Dong, W. Hu, Y. Liu and D. Zhu, *Chem. Rev.*, 2011, **112**, 2208–2267.
- 167 M. Gross, D. C. Müller, H.-G. Nothofer, U. Scherf, D. Neher, C. Bräuchle and K. Meerholz, *Nature*, 2000, **405**, 661.
- 168 C. Wu, M. Lu, S. Chang and C. Wei, *Adv. Funct. Mater.*, 2007, **17**, 1063–1070.
- 169 S. A. Sapp, G. A. Sotzing and J. R. Reynolds, *Chem. Mater.*, 1998, **10**, 2101–2108.
- 170 S. A. Sapp, G. A. Sotzing, J. L. Reddinger and J. R. Reynolds, *Adv. Mater.*, 1996, **8**, 808–811.
- 171 G. Gunbas and L. Toppare, *Chem. Commun.*, 2012, **48**, 1083–1101.
- 172 R. J. Mortimer, D. R. Rosseinsky and P. M. S. Monk, *Electrochromic materials and devices*, John Wiley & Sons, 2015.
- 173 J. Heinze, B. A. Frontana-Uribe and S. Ludwigs, *Chem. Rev.*, 2010, **110**, 4724–4771.
- 174 J. Rivnay, S. Inal, B. A. Collins, M. Sessolo, E. Stavrinidou, X. Strakosas, C. Tassone, D. M. DeLongchamp and G. G. Malliaras, *Nat. Commun.*, 2016, **7**, 11287.
- 175 A. O. Patil, A. J. Heeger and F. Wudl, *Chem. Rev.*, 1988, **88**, 183–200.
- 176 L. M. Tolbert, *Acc. Chem. Res.*, 1992, **25**, 561–568.
- 177 J. L. Bredas and G. B. Street, *Acc. Chem. Res.*, 1985, **18**, 309–315.
- 178 F. A. Arroyave and J. R. Reynolds, *Macromolecules*, 2012, **45**, 5842–5849.
- 179 P. Schottland, K. Zong, C. L. Gaupp, B. C. Thompson, C. A. Thomas, I. Giurgiu, R. Hickman, K. A. Abboud and J. R. Reynolds, *Macromolecules*, 2000, **33**, 7051–7061.
- 180 B. D. Reeves, B. C. Thompson, K. A. Abboud, B. E. Smart and J. R. Reynolds, *Adv. Mater.*, 2002, **14**, 717–719.
- 181 P. M. Beaujuge, C. M. Amb and J. R. Reynolds, *Acc. Chem. Res.*, 2010, **43**, 1396–1407.
- 182 J. Roncali, *Chem. Rev.*, 1992, **92**, 711–738.
- 183 J.-R. Pouliot, F. Grenier, J. T. Blaskovits, S. Beaupré and M. Leclerc, *Chem. Rev.*, 2016, **116**, 14225–14274.
- 184 A. L. Dyer, A. M. Österholm, D. E. Shen, K. E. Johnson and J. R. Reynolds, in *Electrochromic Materials and Devices*, ed. R. J. Mortimer, D. R. Rosseinsky and P. M. S. Monk, Wiley-VCH Verlag GmbH & Co. KGaA, Germany, 1st edn, 2015, ch. 5, pp. 113–183.
- 185 R. J. Mortimer, A. L. Dyer and J. R. Reynolds, *Displays*, 2006, **27**, 2–18.
- 186 L. Groenendaal, G. Zotti, P. Aubert, S. M. Waybright and J. R. Reynolds, *Adv. Mater.*, 2003, **15**, 855–879.
- 187 I. D. Brotherston, D. S. K. Mudigonda, J. M. Osborn, J. Belk, J. Chen, D. C. Loveday, J. L. Boehme, J. P. Ferraris and D. L. Meeker, *Electrochim. Acta*, 1999, **44**, 2993–3004.
- 188 H.-J. Yen and G.-S. Liou, *Polym. Chem.*, 2012, **3**, 255–264.
- 189 C. L. Chochos and S. A. Choulis, *Prog. Polym. Sci.*, 2011, **36**, 1326–1414.
- 190 A. Patra, M. Bendikov and S. Chand, *Acc. Chem. Res.*, 2014, **47**, 1465–1474.
- 191 R. M. Walczak and J. R. Reynolds, *Adv. Mater.*, 2006, **18**, 1121–1131.
- 192 A. L. Dyer, M. R. Craig, J. E. Babiarz, K. Kiyak and J. R. Reynolds, *Macromolecules*, 2010, **43**, 4460–4467.
- 193 C. L. Gaupp and J. R. Reynolds, *Macromolecules*, 2003, **36**, 6305–6315.
- 194 B. D. Reeves, C. R. G. Grenier, A. A. Argun, A. Cirpan, T. D. McCarley and J. R. Reynolds, *Macromolecules*, 2004, **37**, 7559–7569.
- 195 J. A. Kerszulis, K. E. Johnson, M. Kuepfert, D. Khoshabo, A. L. Dyer and J. R. Reynolds, *J. Mater. Chem. C*, 2015, **3**, 3211–3218.
- 196 A. Kumar, D. M. Welsh, M. C. Morvant, F. Piroux, K. A. Abboud and J. R. Reynolds, *Chem. Mater.*, 1998, **10**, 896–902.
- 197 B. Sankaran and J. R. Reynolds, *Macromolecules*, 1997, **30**, 2582–2588.
- 198 A. Kumar and J. R. Reynolds, *Macromolecules*, 1996, **29**, 7629–7630.
- 199 Q. Pei, G. Zuccarello, M. Ahlskog and O. Inganäs, *Polymer*, 1994, **35**, 1347–1351.
- 200 J. C. Gustafsson, B. Liedberg and O. Inganäs, *Solid State Ionics*, 1994, **69**, 145–152.
- 201 C. A. Cutler, M. Bouguettaya and J. R. Reynolds, *Adv. Mater.*, 2002, **14**, 684–688.

- 202 J. Kim, J. You, B. Kim, T. Park and E. Kim, *Adv. Mater.*, 2011, **23**, 4168–4173.
- 203 J. F. Ponder Jr, A. M. Österholm and J. R. Reynolds, *Macromolecules*, 2016, **49**, 2106–2111.
- 204 C. L. Gaupp, D. M. Welsh and J. R. Reynolds, *Macromol. Rapid Commun.*, 2002, **23**, 885–889.
- 205 D. M. Welsh, L. J. Kloeppner, L. Madrigal, M. R. Pinto, B. C. Thompson, K. S. Schanze, K. A. Abboud, D. Powell and J. R. Reynolds, *Macromolecules*, 2002, **35**, 6517–6525.
- 206 B. D. Reeves, E. Unur, N. Ananthakrishnan and J. R. Reynolds, *Macromolecules*, 2007, **40**, 5344–5352.
- 207 M. Dietrich, J. Heinze, G. Heywang and F. Jonas, *J. Electroanal. Chem.*, 1994, **369**, 87–92.
- 208 A. Cirpan, A. A. Argun, C. R. G. Grenier, B. D. Reeves and J. R. Reynolds, *J. Mater. Chem.*, 2003, **13**, 2422–2428.
- 209 K. Krishnamoorthy, A. V. Ambade, M. Kanungo, A. Q. Contractor and A. Kumar, *J. Mater. Chem.*, 2001, **11**, 2909–2911.
- 210 J. Mei and Z. Bao, *Chem. Mater.*, 2013, **26**, 604–615.
- 211 D. T. Christiansen and J. R. Reynolds, *Macromolecules*, 2018, **51**, 9250–9258.
- 212 C. M. Amb, J. A. Kerszulis, E. J. Thompson, A. L. Dyer and J. R. Reynolds, *Polym. Chem.*, 2011, **2**, 812–814.
- 213 J. A. Kerszulis, C. M. Amb, A. L. Dyer and J. R. Reynolds, *Macromolecules*, 2014, **47**, 5462–5469.
- 214 C. M. Amb, P. M. Beaujuge and J. R. Reynolds, *Adv. Mater.*, 2010, **22**, 724–728.
- 215 P. M. Beaujuge, S. V. Vasilyeva, S. Ellinger, T. D. McCarley and J. R. Reynolds, *Macromolecules*, 2009, **42**, 3694–3706.
- 216 P. Shi, C. M. Amb, E. P. Knott, E. J. Thompson, D. Y. Liu, J. Mei, A. L. Dyer and J. R. Reynolds, *Adv. Mater.*, 2010, **22**, 4949–4953.
- 217 S. Ming, S. Zhen, K. Lin, L. Zhao, J. Xu and B. Lu, *ACS Appl. Mater. Interfaces*, 2015, **7**, 11089–11098.
- 218 L. You, J. He and J. Mei, *Polym. Chem.*, 2018, **9**, 5262–5267.
- 219 A. Durmus, G. E. Gunbas and L. Toppare, *Chem. Mater.*, 2007, **19**, 6247–6251.
- 220 P. Camurlu, *RSC Adv.*, 2014, **4**, 55832–55845.
- 221 D. T. Christiansen, D. L. Wheeler, A. L. Tomlinson and J. R. Reynolds, *Polym. Chem.*, 2018, **9**, 3055–3066.
- 222 M. Sezgin, O. Ozay, S. Koyuncu, H. Ozay and F. B. Koyuncu, *Chem. Eng. J.*, 2015, **274**, 282–289.
- 223 Y. Li and T. Michinobu, *J. Polym. Sci., Part A: Polym. Chem.*, 2012, **50**, 2111–2120.
- 224 H. Yen, C. Chen and G. Liou, *Adv. Funct. Mater.*, 2013, **23**, 5307–5316.
- 225 S. Hsiao, G. Liou and H. Wang, *J. Polym. Sci., Part A: Polym. Chem.*, 2009, **47**, 2330–2343.
- 226 C.-W. Chang, C.-H. Chung and G.-S. Liou, *Macromolecules*, 2008, **41**, 8441–8451.
- 227 G.-S. Liou and H.-Y. Lin, *Macromolecules*, 2008, **42**, 125–134.
- 228 R. L. Elsenbaumer, K. Y. Jen and R. Oboodi, *Synth. Met.*, 1986, **15**, 169–174.
- 229 P. Andersson, D. Nilsson, P. Svensson, M. Chen, A. Malmström, T. Remonen, T. Kugler and M. Berggren, *Adv. Mater.*, 2002, **14**, 1460–1464.
- 230 M. Berggren, D. Nilsson and N. D. Robinson, *Nat. Mater.*, 2007, **6**, 3.
- 231 G. S. Collier, I. Pelse, A. M. Österholm and J. R. Reynolds, *Chem. Mater.*, 2018, **30**, 5161–5168.
- 232 P. M. Beaujuge, C. M. Amb and J. R. Reynolds, *Adv. Mater.*, 2010, **22**, 5383–5387.
- 233 E. E. Havinga, L. W. van Horssen, W. ten Hoeve, H. Wynberg and E. W. Meijer, *Polym. Bull.*, 1987, **18**, 277–281.
- 234 A. O. Patil, Y. Ikenoue, F. Wudl and A. J. Heeger, *J. Am. Chem. Soc.*, 1987, **109**, 1858–1859.
- 235 N. S. Sundaresan, S. Basak, M. Pomerantz and J. R. Reynolds, *J. Chem. Soc., Chem. Commun.*, 1987, 621–622.
- 236 J. F. Ponder, A. M. Österholm and J. R. Reynolds, *Chem. Mater.*, 2017, **29**, 4385–4392.
- 237 L. R. Savagian, A. M. Österholm, J. F. Ponder, K. J. Barth, J. Rivnay and J. R. Reynolds, *Adv. Mater.*, 2018, **30**, 1–6.
- 238 G. S. Collier, I. Pelse and J. R. Reynolds, *ACS Macro Lett.*, 2018, **7**, 1208–1214.
- 239 R. M. Walczak, J. K. Leonard and J. R. Reynolds, *Macromolecules*, 2008, **41**, 691–700.
- 240 F. J. Morin, *Phys. Rev. Lett.*, 1959, **3**, 34.
- 241 E. Dagotto, *Science*, 2005, **309**, 257–262.
- 242 X. Li and R. E. Schaak, *Angew. Chem., Int. Ed.*, 2017, **56**, 15550–15554.
- 243 X. Li and R. E. Schaak, *Chem. Mater.*, 2019, **31**, 2088–2096.
- 244 C. N. Berglund and H. J. Guggenheim, *Phys. Rev.*, 1969, **185**, 1022.
- 245 G. Catalan, *Phase Transitions*, 2008, **81**, 729–749.
- 246 Z. Zhang, D. Schwanz, B. Narayanan, M. Kotiuga, J. A. Dura, M. Cherukara, H. Zhou, J. W. Freeland, J. Li, R. Sutarto, F. He, C. Wu, J. Zhu, Y. Sun, K. Ramadoss, S. S. Nonnenmann, N. Yu, R. Comin, K. M. Rabe, S. K. R. S. Sankaranarayanan and S. Ramanathan, *Nature*, 2018, **553**, 68–72.
- 247 C. R. Wade, M. Li and M. Dincă, *Angew. Chem., Int. Ed.*, 2013, **52**, 13377–13381.
- 248 I. Mjejri, C. M. Doherty, M. Rubio-Martinez, G. L. Drisko and A. Rougier, *ACS Appl. Mater. Interfaces*, 2017, **9**, 39930–39934.
- 249 Q. Jiang, M. Chen, J. Li, M. Wang, X. Zeng, T. Besara, J. Lu, Y. Xin, X. Shan, B. Pan, C. Wang, S. Lin, T. Siegrist, Q. Xiao and Z. Yu, *ACS Nano*, 2017, **11**, 1073–1079.
- 250 P. Salles, D. Pinto, K. Hantanasirisakul, K. Maleski, C. E. Shuck and Y. Gogotsi, *Adv. Funct. Mater.*, 2019, **1809223**, 1–9.
- 251 Y. C. Nah, A. Ghicov, D. Kim, S. Berger and P. Schmuki, *J. Am. Chem. Soc.*, 2008, **130**, 16154–16155.
- 252 H. Wei, X. Yan, Y. Li, S. Wu, A. Wang, S. Wei and Z. Guo, *J. Phys. Chem. C*, 2012, **116**, 4500–4510.
- 253 S. Mishra, S. Lambora, P. Yogi, P. R. Sagdeo and R. Kumar, *ACS Appl. Nano Mater.*, 2018, **1**, 3715–3723.
- 254 F. Lin, D. Nordlund, T. C. Weng, D. Sokaras, K. M. Jones, R. B. Reed, D. T. Gillaspie, D. G. J. Weir, R. G. Moore, A. C. Dillon, R. M. Richards and C. Engrakul, *ACS Appl. Mater. Interfaces*, 2013, **5**, 3643–3649.
- 255 D. M. DeLongchamp and P. T. Hammond, *Adv. Funct. Mater.*, 2004, **14**, 224–232.

- 256 V. Jain, R. Sahoo, J. R. Jinschek, R. Montazami, H. M. Yochum, F. L. Beyer, A. Kumar and J. R. Heflin, *Chem. Commun.*, 2008, 3663–3665.
- 257 J. Zhao, Y. Tian, Z. Wang, S. Cong, D. Zhou, Q. Zhang, M. Yang, W. Zhang, F. Geng and Z. Zhao, *Angew. Chem., Int. Ed.*, 2016, **55**, 7161–7165.
- 258 J. Wang, L. Zhang, L. Yu, Z. Jiao, H. Xie, X. W. Lou and X. Wei Sun, *Nat. Commun.*, 2014, **5**, 1–7.
- 259 D. Wei, M. R. J. Scherer, C. Bower, P. Andrew, T. Ryhänen and U. Steiner, *Nano Lett.*, 2012, **12**, 1857–1862.
- 260 Y. Tian, S. Cong, W. Su, H. Chen, Q. Li, F. Geng and Z. Zhao, *Nano Lett.*, 2014, **14**, 2150–2156.
- 261 M. H. Yeh, L. Lin, P. K. Yang and Z. L. Wang, *ACS Nano*, 2015, **9**, 4757–4765.
- 262 S. K. Deb, S.-H. Lee, C. E. Tracy, J. R. Pitts, B. A. Gregg and H. M. Branz, *Electrochim. Acta*, 2001, **46**, 2125–2130.
- 263 D. E. Shen, A. M. Österholm and J. R. Reynolds, *J. Mater. Chem. C*, 2015, **3**, 9715–9725.
- 264 H. Huang, J. Tian, W. K. Zhang, Y. P. Gan, X. Y. Tao, X. H. Xia and J. P. Tu, *Electrochim. Acta*, 2011, **56**, 4281–4286.
- 265 Q. Liu, Q. Chen, Q. Zhang, Y. Xiao, X. Zhong, G. Dong, M. P. Delplancke-Ogletree, H. Terryn, K. Baert, F. Reniers and X. Diao, *J. Mater. Chem. C*, 2018, **6**, 646–653.
- 266 Y. Ren, W. K. Chim, L. Guo, H. Tanoto, J. Pan and S. Y. Chiam, *Sol. Energy Mater. Sol. Cells*, 2013, **116**, 83–88.
- 267 J. Padilla and T. F. Otero, *Electrochem. Commun.*, 2008, **10**, 1–6.
- 268 S. Wang, F. Li, A. D. Easley and J. L. Lutkenhaus, *Nat. Mater.*, 2019, **18**, 69.
- 269 Y. Takahashi, N. Hayashi, K. Oyaizu, K. Honda and H. Nishide, *Polym. J.*, 2008, **40**, 763.
- 270 J. He, S. Mukherjee, X. Zhu, L. You, B. W. Boudouris and J. Mei, *ACS Appl. Mater. Interfaces*, 2018, **10**, 18956–18963.
- 271 J. Remmele, D. E. Shen, T. Mustonen and N. Fruehauf, *ACS Appl. Mater. Interfaces*, 2015, **7**, 12001–12008.
- 272 S. Hassab and J. Padilla, *Electrochem. Commun.*, 2016, **72**, 87–90.
- 273 Y. Kim, H. Shin, M. Han, S. Seo, W. Lee, J. Na, C. Park and E. Kim, *Adv. Funct. Mater.*, 2017, **27**, 1701192.
- 274 J. He, L. You, D. T. Tran and J. Mei, *ACS Appl. Mater. Interfaces*, 2019, **11**, 4169–4177.
- 275 L. Kong, C. Zhang, J. Wang, W. Qiao, L. Ling and D. Long, *ACS Nano*, 2015, **9**, 11200–11208.
- 276 Z. Tong, N. Li, H. Lv, Y. Tian, H. Qu, X. Zhang, J. Zhao and Y. Li, *Sol. Energy Mater. Sol. Cells*, 2016, **146**, 135–143.
- 277 C. K. Chan, H. Peng, R. D. Twisten, K. Jarausch, X. F. Zhang and Y. Cui, *Nano Lett.*, 2007, **7**, 490–495.
- 278 C. Delmas, H. Cognac-Auradou, J. M. Cocciantelli, M. Menetrier and J. P. Doumerc, *Solid State Ionics*, 1994, **69**, 257–264.
- 279 D. W. Murphy, *J. Electrochem. Soc.*, 2006, **126**, 497.
- 280 K. West, B. Zachau-Christiansen, T. Jacobsen and S. Atlung, *J. Power Sources*, 1985, **14**, 235–245.
- 281 M. R. J. Scherer, L. Li, P. M. S. Cunha, O. A. Scherman and U. Steiner, *Adv. Mater.*, 2012, **24**, 1217–1221.
- 282 Y. Wang, K. Takahashi, K. Lee and G. Cao, *Adv. Funct. Mater.*, 2006, **16**, 1133–1144.
- 283 L. Long, S. Wang, M. Xiao and Y. Meng, *J. Mater. Chem. A*, 2016, **4**, 10038–10039.
- 284 Z. Zhang, Y. Shao, B. Lotsch, Y. S. Hu, H. Li, J. Janek, L. F. Nazar, C. W. Nan, J. Maier, M. Armand and L. Chen, *Energy Environ. Sci.*, 2018, **11**, 1945–1976.
- 285 M. A. Habib, S. P. Maheswari and M. K. Carpenter, *J. Appl. Electrochem.*, 1991, **21**, 203–207.
- 286 P. Jia, W. A. Yee, J. Xu, C. L. Toh, J. Ma and X. Lu, *J. Membr. Sci.*, 2011, **376**, 283–289.
- 287 S. A. Agnihotry, S. Nidhi, P. Pradeep and S. S. Sekhon, *Solid State Ionics*, 2000, **136–137**, 573–576.
- 288 P. Baudry, *J. Electrochem. Soc.*, 2006, **138**, 460.
- 289 H. Li and J. Liang, *Adv. Mater.*, 2019, 1805864, DOI: 10.1002/adma.201805864.
- 290 M. T. Otley, F. A. Alamer, Y. Zhu, A. Singhaviranon, X. Zhang, M. Li, A. Kumar and G. A. Sotzing, *ACS Appl. Mater. Interfaces*, 2014, **6**, 1734–1739.
- 291 M. Dewaele, D. Truffier-Boutry, J. Devaux and G. Leloup, *Dent. Mater.*, 2006, **22**, 359–365.
- 292 K. Dahmouche, M. Atik, N. C. Mello, T. J. Bonagamba, H. Panepucci, M. A. Aegerter, P. Judeinstein, P. H. De Souza, H. Panepucci, S. H. Pulcinelli and C. V. Santilli, *J. Sol-Gel Sci. Technol.*, 1998, **13**, 909–913.
- 293 Y. Xiao, X. Zhong, J. Guo, C. Zhou, H. Zuo, Q. Liu, Q. Huang, Q. Zhang and X. Diao, *Electrochim. Acta*, 2018, **260**, 254–263.
- 294 A. A. Argun, A. Cirpan and J. R. Reynolds, *Adv. Mater.*, 2003, **15**, 1338–1341.
- 295 S. Hashimoto, H. Matsuoka, H. Kagechika, M. Susa and K. S. Goto, *J. Electrochem. Soc.*, 1990, **137**, 1300–1304.
- 296 H. Matsuoka, S. Hashimoto and H. Kagechika, *J. Surf. Finish. Soc. Jpn.*, 2011, **42**, 246–252.
- 297 N. Ozer and C. M. Lampert, *Thin Solid Films*, 1999, **349**, 205–211.
- 298 C. Bechinger, H. Muffler, C. Schäfle, O. Sundberg and P. Leiderer, *Thin Solid Films*, 2000, **366**, 135–138.
- 299 J. Jensen, M. Hösel, A. L. Dyer and F. C. Krebs, *Adv. Funct. Mater.*, 2015, **25**, 2073–2090.
- 300 R. R. Sondergaard, M. Hösel, M. Jørgensen and F. C. Krebs, *J. Polym. Sci., Part B: Polym. Phys.*, 2013, **51**, 132–136.
- 301 J. Jensen, M. Hösel, I. Kim, J. S. Yu, J. Jo and F. C. Krebs, *Adv. Funct. Mater.*, 2014, **24**, 1228–1233.
- 302 W. R. Lian, Y. C. Huang, Y. A. Liao, K. L. Wang, L. J. Li, C. Y. Su, D. J. Liaw, K. R. Lee and J. Y. Lai, *Macromolecules*, 2011, **44**, 9550–9555.
- 303 R. T. Wen, C. G. Granqvist and G. A. Niklasson, *Nat. Mater.*, 2015, **14**, 996–1001.
- 304 M. A. Arvizu, R. T. Wen, D. Primetzhofer, J. E. Klemberg-Sapieha, L. Martinu, G. A. Niklasson and C. G. Granqvist, *ACS Appl. Mater. Interfaces*, 2015, **7**, 26387–26390.
- 305 R. T. Wen, G. A. Niklasson and C. G. Granqvist, *ACS Appl. Mater. Interfaces*, 2016, **8**, 5777–5782.
- 306 D. Dong, W. Wang, A. Rougier, A. Barnabé, G. Dong, F. Zhang and X. Diao, *J. Mater. Chem. C*, 2018, **6**, 9875–9889.

- 307 J. H. Huang, C. Y. Hsu, C. W. Hu, C. W. Chu and K. C. Ho, *ACS Appl. Mater. Interfaces*, 2010, **2**, 351–359.
- 308 S. Guan, A. S. Elmezayyen, F. Zhang, J. Zheng and C. Xu, *J. Mater. Chem. C*, 2016, **4**, 4584–4591.
- 309 B. Gélinas, D. Das and D. Rochefort, *ACS Appl. Mater. Interfaces*, 2017, **9**, 28726–28736.
- 310 H. Shin, S. Seo, C. Park, J. Na, M. Han and E. Kim, *Energy Environ. Sci.*, 2016, **9**, 117–122.
- 311 J. He, L. You and J. Mei, *ACS Appl. Mater. Interfaces*, 2017, **9**, 34122–34130.
- 312 J.-C. Vidal, E. Garcia-Ruiz and J.-R. Castillo, *Microchim. Acta*, 2003, **143**, 93–111.
- 313 J. Heinze, B. A. Frontana-Urbe and S. Ludwigs, *Chem. Rev.*, 2010, **110**, 4724–4771.
- 314 X. Wang, B. Shapiro and E. Smela, *Adv. Mater.*, 2004, **16**, 1605–1609.
- 315 E. Smela and N. Gadegaard, *J. Phys. Chem. B*, 2001, **105**, 9395–9405.
- 316 T. F. Otero and I. Boyano, *J. Phys. Chem. B*, 2003, **107**, 6730–6738.
- 317 G. L. Duffitt and P. G. Pickup, *J. Chem. Soc., Faraday Trans.*, 1992, **88**, 1417–1423.
- 318 M. Zhou, M. Pagels, B. Geschke and J. Heinze, *J. Phys. Chem. B*, 2002, **106**, 10065–10073.
- 319 S. V. Vasilyeva, P. M. Beaujuge, S. Wang, J. E. Babiarz, V. W. Ballarotto and J. R. Reynolds, *ACS Appl. Mater. Interfaces*, 2011, **3**, 1022–1032.
- 320 E. Unur, P. M. Beaujuge, S. Ellinger, J.-H. Jung and J. R. Reynolds, *Chem. Mater.*, 2009, **21**, 5145–5153.
- 321 D. T. Gillaspie, R. C. Tenent and A. C. Dillon, *J. Mater. Chem.*, 2010, **20**, 9585–9592.
- 322 M. Da Rocha, Y. He, X. Diao and A. Rougier, *Sol. Energy Mater. Sol. Cells*, 2018, **177**, 57–65.
- 323 A. Rivaton, A. Tournebize, J. Gaume, P. O. Bussière, J. L. Gardette and S. Therias, *Polym. Int.*, 2014, **63**, 1335–1345.
- 324 J. Jensen, M. V. Madsen and F. C. Krebs, *J. Mater. Chem. C*, 2013, **1**, 4826–4835.
- 325 B.-X. Wei, L. Zhao, T.-J. Wang, H. Gao, H.-X. Wu and Y. Jin, *Adv. Powder Technol.*, 2013, **24**, 708–713.
- 326 S. Hu, N. S. Lewis, J. W. Ager, J. Yang, J. R. McKone and N. C. Strandwitz, *J. Phys. Chem. C*, 2015, **119**, 24201–24228.
- 327 S. D. Tilley, *Adv. Energy Mater.*, 2019, **9**, 1802877.
- 328 D. Bae, B. Seger, P. C. K. Vesborg, O. Hansen and I. Chorkendorff, *Chem. Soc. Rev.*, 2017, **46**, 1933–1954.
- 329 R. H. Bulloch and J. R. Reynolds, *J. Mater. Chem. C*, 2016, **4**, 603–610.
- 330 X. Cai, T. Lei, D. Sun and L. Lin, *RSC Adv.*, 2017, **7**, 15382–15389.